Asymptotic identification uncertainty of well-separated modes in operational modal analysis with multiple setups

Yan-Long Xie [a], Siu-Kui Au [b], Binbin Li [a,c*]

[a] ZJU-UIUC Institute, Zhejiang University, China

[b] School of Civil and Environmental Engineering, Nanyang Technological University, Singapore

[c] College of Civil Engineering and Architecture, Zhejiang University, China

Abstract

Operational modal analysis (OMA) aims at identifying structural modal properties with (output-only) ambient vibration data. In the absence of loading information, the identification (ID) uncertainty of modal properties becomes a valid concern in quality control and test planning. One recent development that addresses this aspect is 'uncertainty law', which aims at understanding how ID uncertainty depends on test configuration. Mathematically, uncertainty laws in OMA are asymptotic expressions for the 'posterior' (i.e., given data) variance of modal parameters. Analogous to the laws of large numbers in statistics, they are often derived assuming long data, small damping, and high signal-to-noise ratio. Following a Bayesian approach, this work develops the uncertainty law for OMA with multiple setup data, a common strategy to produce a 'global' mode shape covering a large number of locations with a small number of sensors in individual setups. It advances over previous results for single setup data, and is motivated by questions, e.g., how does the quality of global mode shape depend on sensor locations and setup schedule? Focusing on the case of fixed reference and distinct rovers, analytical study of the eigenvalue properties of mode shape covariance matrix reveals characteristic spatial patterns where principal uncertainty takes place, which can be of local or global nature. The theory is validated with synthetic, laboratory and field test data. By virtue of the Cramer-Rao bound, up to the same modeling assumptions, the uncertainty law dictates the achievable precision limit of OMA regardless of identification method.

Keywords: BAYOMA; Cramer-Rao Bound; Operational modal analysis; Uncertainty law; Multiple setup.

1 Introduction

Structural modal parameters primarily include natural frequencies, damping ratios, and mode shapes. 'Operational modal analysis' (OMA) [1,2] aims at identifying them using 'output-only' ambient vibration response data. For its economy in implementation, OMA has attracted considerable attention in field testing of civil engineering structures [3–7]. Common downstream applications include model updating [8,9], damage detection [10,11], and more generally, structural health monitoring [12–14]. In OMA, there are many situations where the number of synchronous data channels is smaller than the number of degrees of freedom (DOFs) for a mode shape of required spatial resolution, often limited by the number of sensors, data acquisition hardware or logistics. This calls for a 'multiple setup' strategy, where sensors are 'roved' to cover different DOFs in different setups. 'Reference sensors' are present to measure DOFs shared by different setups, effectively providing a common scaling for 'gluing' local mode shape information into a 'global mode shape' covering all desired DOFs [15–18].

In the absence of loading information, the identification (ID) uncertainty in OMA becomes a valid concern [17,19]. With multiple setup data the ID uncertainty of local mode shapes can propagate into the global mode shape, which can be influenced by the choice of reference and rover sensor locations/schedules. It is therefore of interest to assess the ID uncertainty and investigate how it depends on test configuration. Conventionally, uncertainty quantification can be approached from either a classical statistical ('frequentist') or a Bayesian perspective. In a frequentist context, ID uncertainty refers to the ensemble variance of modal estimates under hypothetical repeated experiments [19,20]. For example, for stochastic subspace identification (SSI), methods based on first-order perturbation are available for single setup data [19] and multiple setup data [21]. Methods are also available for frequency domain maximum likelihood approach [22,23]. The past decade has seen developments in Bayesian operational modal analysis (BAYOMA) [24], where, under a Gaussian approximation of the 'posterior' (i.e., given data) distribution, ID results are characterized in terms of the posterior most probable value (MPV) and covariance matrix [9]. Among others, a frequency domain formulation based on the FFT of data in a selected resonance band of the target mode(s) is found to be attractive in terms of model robustness and computational efficiency; see Section 10.2 of [24]. For well-separated modes, computational strategies have been developed for single setup data [25] and multiple setup data [26,27].

Being able to calculate ID uncertainty by itself does not provide much insight into what factors it depends on. Due to the complicated nature of the inverse problem, it is unlikely that one can express the ID uncertainty analytically in an exact form and applicable to general situations. Focusing on well-separated modes in a single setup context, for long data, small damping, and high modal signal-to-noise (s/n) ratio, asymptotic expressions for the leading order posterior c.o.v. (coefficient of variation = standard derivation/mean) have been derived in an explicit closed form. They are collectively referred as 'uncertainty law', analogous to laws of large numbers in statistics. They comprise a 'zeroth-order law' that gives the achievable precision for noiseless data [28] and a 'first-order law' that accounts for the effect of 'modal s/n ratio' (see (4) later), which is a fundamental parameter capturing test configuration [29]. Applications in field test planning can be found in [30,31]. Uncertainty law for close modes identified with single setup data has been recently developed [32–34].

To understand how the ID quality of global mode shape depends on test configuration, this work develops the uncertainty law for OMA with multiple setup data. The major task lies in analytical investigation of the posterior covariance matrix of modal parameters under the stated asymptotic conditions. In what follows, Section 2 gives a brief review of Bayesian OMA incorporating multiple setup data. Section 3 summarizes the key results, which will be derived in Section 4 and verified in Section 5 (synthetic data) and Section 6 (laboratory and field data). Concluding remarks are given in Section 7.

2 Bayesian OMA with multiple setup data

Consider modal ID of a structure using ambient acceleration data from n_s setups at different time periods, each covering a possibly different set of DOFs. Let $\{\ddot{\boldsymbol{y}}_{ij}\}_{j=0}^{N_i-1}$ (each $n_i \times 1$) be the data in Setup i sampled at time interval Δt_i (sec), where n_i is the number of data channels and N_i is the number of samples per channel. The (scaled one-sided) FFT of $\{\ddot{\boldsymbol{y}}_{ij}\}_{j=0}^{N_i-1}$ at frequency $\mathrm{f}_{ik} = k/N_i\Delta t_i$ (Hz, up to Nyquist frequency) is defined as

$$F_{ik} = \sqrt{\frac{2\Delta t_i}{N_i}} \sum_{j=0}^{N_i-1} \ddot{\boldsymbol{y}}_{ij} e^{-2\pi \mathbf{i} jk/N} \tag{1}$$

where $\mathbf{i}^2 = -1$. For a classically damped structural mode well-separated from others, the FFT data within a selected resonance band is modeled as $F_{ik} = \boldsymbol{\nu}_i \ddot{\eta}_{ik} + \boldsymbol{\varepsilon}_{ik}$, where $\boldsymbol{\varepsilon}_{ik}$ ($n_i \times 1$) is

the channel noise, $\boldsymbol{v}_i$ $(n_i \times 1)$ is local mode shape confined to n_i measured DOFs, and $\ddot{\eta}_{ik}$ is the scaled FFT of theoretical modal acceleration response. The time-domain counterpart of $\ddot{\eta}_{ik}$ satisfies $\ddot{\eta}_i + 2\zeta_i\omega_i\dot{\eta}_i + \omega_i^2\eta_i = p_i$, where (for Setup i) $\omega_i = 2\pi f_i$ (rad/sec) and f_i (Hz) is the natural frequency, ζ_i is the damping ratio and p_i is the modal force per unit modal mass. The modal force and channel noise are assumed to be stochastic stationary with constant power spectral density (PSD) within the selected frequency band, denoted by S_i and S_{e_i}, respectively.

As the setups are performed at different time periods where modal properties and environment can possibly change, $\{f_i, \zeta_i, S_i, S_{e_i}\}$ in different setups are parameterized separately. The only property that is common to the setups is the 'global mode shape' $\boldsymbol{\varphi}$ $(n \times 1)$, where n is the total number of distinct DOFs from all setups. It is related to the local mode shape by $\boldsymbol{v}_i = \boldsymbol{L}_i\boldsymbol{\varphi}$, where $\boldsymbol{L}_i$ $(n_i \times n)$ is a selection matrix, with $\boldsymbol{L}_i(j,k) = 1$ if data channel j in Setup i measures DOF k in $\boldsymbol{\varphi}$; and zero otherwise.

Let $\boldsymbol{\theta}$ comprise the parameters from all setups, i.e., $\{f_i\}_{i=1}^{n_s}$, $\{\zeta_i\}_{i=1}^{n_s}$, $\{S_i\}_{i=1}^{n_s}$, $\{S_{e_i}\}_{i=1}^{n_s}$ and $\boldsymbol{\varphi}$. It will be identified using the FFT data from all setups, i.e., $D = \{D_i\}_{i=1}^{n_s}$, where $D_i = \{F_{ik}\}$ denotes the FFTs in the selected band of Setup i. The global mode shape is scaled to have unit norm, i.e., $\|\boldsymbol{\varphi}\|^2 = \boldsymbol{\varphi}^T\boldsymbol{\varphi} = 1$. The modal force PSDs $\{S_i\}_{i=1}^{n_s}$ correspond to this common scaling. In a Bayesian approach, the ID result about $\boldsymbol{\theta}$ given data D is encapsulated in the posterior probability density function (PDF) $p(\boldsymbol{\theta}|D)$. Using Bayes' Theorem with a uniform prior distribution for $\boldsymbol{\theta}$, $p(\boldsymbol{\theta}|D) \propto p(D|\boldsymbol{\theta}) = \exp[-L(D;\boldsymbol{\theta})]$, where $L(D;\boldsymbol{\theta}) = -ln[p(D|\boldsymbol{\theta})]$ is the 'negative log-likelihood function' (NLLF) often used for analysis. In the present context, given $\boldsymbol{\theta}$ the data in different setups are independent and so $L = \sum_{i=1}^{n_s} L_i$ where $L_i = -\ln p(D_i|\boldsymbol{\theta})$ is the NLLF of Setup i. With stochastic stationary data assumed in each setup, standard theory [35] (see also Section 4.8.3 of [24]) shows that for sufficiently long data the F_{ik}s are independent for different frequencies (indexed by k) and each has a (circularly symmetric) complex Gaussian distribution, i.e.,

$$L_i = n_i N_{fi} ln\pi + \sum_k \ln|\boldsymbol{E}_{ik}| + \sum_k F_{ik}^* \boldsymbol{E}_{ik}^{-1} F_{ik} \tag{2}$$

where the sums are over the N_{fi} FFT points in the selected band of Setup i;

$$\boldsymbol{E}_{ik} = S_i D_{ik} \boldsymbol{v}_i \boldsymbol{v}_i^T + S_{e_i} \boldsymbol{I} \tag{3}$$

is the theoretical PSD matrix of data. Here, $D_{ik} = \left[\left(1-\beta_{ik}^2\right)^2 + (2\zeta_i\beta_{ik})^2\right]^{-1}$ is the dynamic amplification between the modal force PSD and modal acceleration response PSD, with $\beta_{ik} = \mathrm{f}_{ik}/f_i$ (ratio of FFT frequency to natural frequency). Throughout this work, $\boldsymbol{I}$ and $\boldsymbol{0}$ denote respectively an identity matrix and zero matrix of legitimate size. In typical cases with sufficient data, the posterior PDF of $\boldsymbol{\theta}$ can be approximated by a Gaussian PDF centered at the MPV, which is the location where the NLLF is minimized. The covariance matrix of the PDF quantifies ID uncertainty for given data. It is equal to the inverse of Hessian matrix of the NLLF at the MPV. The above context is the same as in previous work [26,27] of BAYOMA for multiple setup data.

3 Overview of key results

The posterior covariance matrix of modal parameters can be calculated for a given set of data, but the numerical value does not offer insights about how it depends on the test configuration. 'Uncertainty law' addresses this question by studying the large sample size behavior of the covariance matrix, assuming that the data is indeed distributed as the likelihood function for some 'true' parameters (assumed to exist). This 'frequentist' assumption is introduced to achieve the objective of uncertainty law, i.e., understanding and planning. As with any inference or prediction methodology, uncertainty law does not account for modeling error beyond stated assumptions. For the ease of reading, the key results of the work are summarized in this section. They will be derived in Section 4 and verified/illustrated in Section 5 and Section 6 later.

For each Setup i, let the selected frequency band be specified as $f_i(1 \pm \kappa_i\zeta_i)$, where κ_i is a dimensionless bandwidth factor, e.g., $\kappa_i = 1$ corresponds to the half power band. Assuming a data duration of $T_{di} = N_i\Delta t_i$ (sec), the band has $N_{fi} = 2\kappa_i\zeta_i f_i T_{di}$ FFT points separated by $\Delta\mathrm{f} = 1/T_{di}$ (Hz). The results to be presented here are derived in the context of Section 2 and under the asymptotic conditions of (for all setups $i = 1, \ldots, n_s$) long data ($N_{fi} \gg 1$), small damping ($\zeta_i \ll 1$) and high modal s/n ratio ($\gamma_i \gg 1$):

$$\gamma_i = \frac{S_i\|\boldsymbol{v}_i\|^2}{4S_{e_i}\zeta_i^2} \tag{4}$$

These asymptotic conditions are introduced so that the problem is mathematically tractable to yield explicit expressions for gaining insights and test planning. They are the same as those

used previously in deriving the uncertainty law for single setup data [28,29], now imposed for all setups. Additional assumptions on setup configurations (fixed reference and distinct rovers) are introduced later to develop results with deeper insights on mode shape uncertainty.

3.1 Parameters other than mode shapes

We show that, except for mode shape, the parameters of different setups are uncorrelated. For each Setup i, these parameters include the natural frequency f_i, damping ratio ζ_i, modal force PSD S_i and channel noise PSD S_{e_i}. They are all uncorrelated from mode shape, be it local ($\boldsymbol{v}_i$) or global ($\boldsymbol{\varphi}$). Their covariance matrix is the same as the one with only single setup data, where specific formula can be found in Section 4 of [29] or Section 15.1 of [24]. These findings of decorrelation are not surprising, because the data in different setups are connected through their local mode shape only, but which (from early work [29]) are asymptotically uncorrelated from the remaining parameters, i.e., data from other setups do not help.

3.2 Mode shape uncertainty, general situation

The important and interesting discovery in this work lies in the uncertainty of global mode shape $\boldsymbol{\varphi}$. We show that the posterior covariance matrix of $\boldsymbol{\varphi}$ is asymptotically given by

$$\boldsymbol{C}_{\varphi\varphi} \sim \boldsymbol{J}^{+} \tag{5}$$

where the superscripted '+' denotes a pseudo-inverse, i.e., ignoring the zero eigenvalue due to the mode shape norm constraint;

$$\boldsymbol{J} = \sum_i k_i \boldsymbol{L}_i^T \left(\boldsymbol{I} - \overline{\boldsymbol{v}}_i \overline{\boldsymbol{v}}_i^T\right) \boldsymbol{L}_i \tag{6}$$

is the asymptotic expression of $\partial^2 L/\partial \varphi^2$; $\overline{\boldsymbol{v}}_i = \|\boldsymbol{v}_i\|^{-1} \boldsymbol{v}_i$ is the local mode shape scaled to have unit norm locally (i.e., $\|\overline{\boldsymbol{v}}_i\| = 1$), to be distinguished from the local mode shape $\boldsymbol{v}_i$ that is scaled globally ($\|\boldsymbol{\varphi}\| = 1$);

$$k_i = \frac{S_i}{S_{e_i}\zeta_i} N_{ci} \tan^{-1} \kappa_i \tag{7}$$

is a dimensionless parameter that quantifies mode shape ID precision in Setup i; $N_{ci} = N_i \Delta t f_i$ is a dimensionless duration of Setup i as a multiple of natural period ($1/f_i$ sec).

3.3 Mode shape uncertainty, fixed reference and distinct rovers

While (6) is applicable for general setup schedule, more insightful results can be obtained by narrowing the scope to the situation where the reference DOFs are fixed in all setups and the rover DOFs in different setups are distinct. An additional (somewhat technical) assumption is that in any given setup a DOF is measured by at most one data channel. These assumptions lead to some loss of generality, but they are still common in practice, e.g., fixed reference saves logistics and human error. Under these assumptions, we have obtained analytically the eigenvalue properties of $\boldsymbol{J}$, as summarized in Table 1. The global mode shape covariance matrix $\boldsymbol{C}_{\varphi\varphi}$ has the same set of eigenvectors and its eigenvalues are reciprocals of those of $\boldsymbol{J}$ (except zero eigenvalue). The eigenvectors give the mutually uncorrelated principal directions where ID uncertainty of mode shape takes place. As seen in Table 1, the principal uncertainty can appear in a 'local' (R and V) or 'global' (G) manner. The former has a localized pattern in the eigenvectors and their eigenvalues are simple functions of the k_is. Type R involves the reference DOFs only. Type V involves only the rover DOFs in a particular setup. Type G involves all DOFs in a non-trivial manner, taking the same local shape as R and V but with different proportions determined by an eigenvalue problem. It is the only type that depends on sensor location, through the partial mode shape norms of reference DOFs ($c_R = \|\boldsymbol{u}_R\|^2$) and rover DOFs ($c_i = \|\boldsymbol{u}_i\|^2$).

Table 1 Eigenvalue properties of $\boldsymbol{J}$ (asymptotic form of $\partial^2 L/\partial\varphi^2$). Global mode shape is partitioned as $\boldsymbol{\varphi} = [\boldsymbol{u}_R; \boldsymbol{u}_1; \cdots; \boldsymbol{u}_{n_s}]$, $\boldsymbol{u}_R$ ($n_R \times 1$) for reference DOFs and $\boldsymbol{u}_i$ ($n_{vi} \times 1$) for rover DOFs in Setup i.

Type/nature	Eigenvalue(s)	Eigenvector(s)
N Norm constraint	0	$\boldsymbol{\varphi} = \begin{bmatrix} \boldsymbol{u}_R \\ \boldsymbol{u}_1 \\ \vdots \\ \boldsymbol{u}_{n_s} \end{bmatrix}$, $\|\boldsymbol{\varphi}\|^2 = \|\boldsymbol{u}_R\|^2 + \Sigma_i\|\boldsymbol{u}_i\|^2 = 1$
R Local, reference DOFs	$(n_R - 1)$ eigenvalues, all equal to $\Sigma_i k_i$	Of the form $\begin{bmatrix} \boldsymbol{u}'_R \\ \boldsymbol{0} \\ \vdots \\ \boldsymbol{0} \end{bmatrix}$, where $\boldsymbol{u}'_R$ lies in the $(n_R - 1)$-dimensional orthogonal complement of $\boldsymbol{u}_R$, i.e., $\boldsymbol{u}_R^T\boldsymbol{u}'_R = 0$. The $(n_R - 1)$ possibilities of $\boldsymbol{u}'_R$ are orthogonal
V Local,	For Setup i, $(n_{vi} - 1)$ eigenvalues, all equal to k_i; $i = 1, \dots, n_s$	Of the form $\begin{bmatrix} \boldsymbol{0} \\ \boldsymbol{u}'_1 \\ \boldsymbol{0} \\ \vdots \\ \boldsymbol{0} \end{bmatrix}, \dots, \begin{bmatrix} \boldsymbol{0} \\ \boldsymbol{0} \\ \boldsymbol{0} \\ \vdots \\ \boldsymbol{u}'_{n_s} \end{bmatrix}$ for Setups $i = 1, \dots, n_s$, respectively. For each Setup i, $\boldsymbol{u}'_i$ lies in the $(n_{vi} - 1)$-dimensional orthogonal

rover DOFs		complement of $\boldsymbol{u}_i$, i.e., $\boldsymbol{u}_i^T \boldsymbol{u}_i' = 0$. The $(n_{vi} - 1)$ possibilities of $\boldsymbol{u}_i'$ are orthogonal
G Global, all DOFs	n_s eigenvalues; manageable expressions not yet found, but the sum of eigenvalues is equal to $\Sigma_i k_i$	Of the form $\boldsymbol{x} = \begin{bmatrix} a_R \boldsymbol{u}_R \\ a_1 \boldsymbol{u}_1 \\ \vdots \\ a_{n_s} \boldsymbol{u}_{n_s} \end{bmatrix}$, where $\boldsymbol{a} = \begin{bmatrix} a_R \\ a_1 \\ \vdots \\ a_{n_s} \end{bmatrix}$ satisfies $\boldsymbol{Da} = \lambda \boldsymbol{Ca}$ ($\lambda \neq 0$) as in (38), i.e., the generalized eigenvector with non-zero eigenvalue. There are n_s solutions of $\boldsymbol{a}$ and their corresponding $\boldsymbol{x}$'s are orthogonal

Mode shape is a vector subjected to scaling constraint. One scalar measure of mode shape uncertainty analogous to the c.o.v. of a scalar variable is the 'mode shape c.o.v.', defined as the square root sum of eigenvalues of the mode shape covariance matrix under unit norm constraint; see, e.g., Section 11.3 of [24]. The mode shape c.o.v. can be viewed approximately as the standard deviation of the hyper angle (in radian) between the uncertain and most probable mode shape, which is invariant to the scaling of mode shape.

Further to the eigenvalue properties in Table 1, we have obtained the contributions to the global mode shape c.o.v. (squared) from different principal uncertainties, as summarized in Table 2. Since the principal uncertainties are mutually uncorrelated, their contributions can be simply summed to give the total mode shape c.o.v. (squared), as indicated in the bottom row of the table. Manageable expression for type G eigenvalues of $\boldsymbol{J}$ has not been found but it is still possible to determine the sum of their reciprocals that gives the contribution to mode shape c.o.v.; see Section 4.7 for details. When there is only one setup ($n_s = 1$), the results in Table 1 and Table 2 reduce to those found previously for single setup data [28]. In particular, the eigenvalues of Type R, V and G are all equal to k_1^{-1}. Their eigenvectors form an orthogonal basis in the $(n-1)$-dimensional orthogonal complement of $\boldsymbol{\varphi}$.

Table 2 Contributions to c.o.v. (squared) of global mode shape $\boldsymbol{\varphi} = [\boldsymbol{u}_R; \boldsymbol{u}_1; \dots; \boldsymbol{u}_{n_s}]$ from different types of principal uncertainty; $c_R = \|\boldsymbol{u}_R\|^2$, $c_i = \|\boldsymbol{u}_i\|^2$ $(i = 1, \dots, n_s)$

Type	Nature	Contribution to global mode shape c.o.v. (squared)
N	Norm constraint	0
R	Local, reference DOFs	$\delta_R^2 = (n_R - 1)(\Sigma_i k_i)^{-1}$
V	Local, rover DOFs	$\delta_V^2 = \Sigma_i (n_{vi} - 1) k_i^{-1}$
G	Global, all DOFs	$\delta_G^2 = \Sigma_i k_i^{-1} + \Sigma_{i<j} \frac{c_i c_j}{c_R} (k_i^{-1} + k_j^{-1})$
Total		$\delta_\varphi^2 = \delta_R^2 + \delta_V^2 + \delta_G^2$

3.3.1 Bounds on mode shape c.o.v.

As mentioned earlier, only type G uncertainty depends on sensor location through the partial mode shape norms $c_R = \|\boldsymbol{u}_r\|^2$ and $c_i = \|\boldsymbol{u}_i\|^2$ $(i = 1, \dots, n_s)$. As a result of norm constraint $\|\boldsymbol{\varphi}\| = 1$, they satisfy $c_R + \sum_i c_i = 1$. For fixed c_R, by studying the extreme values of δ_G^2 among all $\{c_i\}_{i=1}^{n_s}$ satisfying this constraint, we show that

$$\sum_i k_i^{-1} \le \delta_G^2 \le \sum_i k_i^{-1} + \frac{1}{2Q}\left(c_R + \frac{1}{c_R} - 2\right) \qquad \text{(fixed reference, distinct rovers)} \qquad (8)$$

where Q is the sum of all entries of $\boldsymbol{A}^{-1}$; $\boldsymbol{A}$ is a $n_s \times n_s$ matrix with entries $\boldsymbol{A}(i,i) = 0$ and $\boldsymbol{A}(i,j) = k_i^{-1} + k_j^{-1}$, $i = 1, \dots, n_s, i \neq j$. The lower bound in (8) is the tightest possible one because it can be reached by picking an arbitrary i and setting $c_j = 0$ $(j \neq i)$. The upper bound corresponds to the global maximum $\hat{\boldsymbol{c}} = \left[\hat{c}_1, \dots, \hat{c}_{n_s}\right]^T$ of δ_G^2, where each $\hat{c}_i$ is equal to the sum of the ith row of $\boldsymbol{A}^{-1}$ multiplied by $(1 - c_R)/Q$. If $0 \le \hat{c}_i \le 1$ for all $i = 1, \dots, n_s$ then the upper bound is achievable and hence is the tightest possible one. See Section 4.8 for details. Substituting the bounds in (8) into $\delta^2 = \delta_R^2 + \delta_V^2 + \delta_G^2$ gives the bounds for the mode shape c.o.v. δ^2 with the same tightness.

As a remark, the lower bound in (8) does not account for practical constraints on the number of sensors, the locations they together must cover, logistics, etc. In reality, these constraints will narrow the range of values of δ_G^2 (and hence δ^2) among candidate setup choices. How to incorporate these constraints depends on the application; discrete/combinatorial type of approach is often more effective. The lower bound does not offer solution to optimal sensor location; the corresponding setup (rovers in only one setup) is clearly against the objective of multiple setups. At the other extreme, the upper bound in (8) is unlikely one that will be intentionally pursued but its upper bound nature offers a simple conservative means for checking whether a candidate setup choice has acceptable global mode shape uncertainty; and to control (if necessary) through a single parameter c_R. It can be reasoned that the upper bound decreases monotonically from ∞ at $c_R = 0$ to the lower bound value $\Sigma_i k_i^{-1}$ (with zero slope) at $c_R = 1$.

4 Theory

In this section we present the mathematical theory supporting the results presented in Section 3. Recall from Section 2 that the set of all modal parameters $\boldsymbol{\theta}$ comprises the natural frequencies $\{f_i\}_{i=1}^{n_s}$, damping ratios $\{\zeta_i\}_{i=1}^{n_s}$, modal force PSDs $\{S_i\}_{i=1}^{n_s}$, channel noise PSDs $\{S_{e_i}\}_{i=1}^{n_s}$ and global mode shape $\boldsymbol{\varphi}$. The latter is subjected to norm constraint $\|\boldsymbol{\varphi}\| = 1$ and $\{S_i\}_{i=1}^{n_s}$ correspond to this common scaling. The covariance matrix of $\boldsymbol{\theta}$ is the inverse of Hessian matrix of the NLLF $L = \Sigma_i L_i$ (satisfying the norm constraint), where L_i is the NLLF of Setup i as given in (2). For notational simplicity, unless otherwise stated Σ_i denotes a sum over i from 1 to n_s. Clearly, $\partial^2 L/\partial\theta^2 = \sum_i \partial^2 L_i/\partial\theta^2$. We will investigate the asymptotic behavior of $\partial^2 L/\partial\theta^2$ by leveraging on previous findings for single setup data [28,29], which is intimately related to the behavior of the individual $\partial^2 L_i/\partial\theta^2$. Alternatively, one can also approach based on the Fisher Information Matrix to derive the asymptotic expressions for the entries in the Hessian matrix [36]. Such approach is applicable for general situations and has been performed in [37] (see Chapter 4), yielding the same result in Sections 3.1 and 3.2.

The NLLF L_i in (2) and the data PSD $\boldsymbol{E}_{ik}$ in (3) have the same form for single setup data, except for one important difference that the local mode shape $\boldsymbol{v}_i$ does not have unit norm. However, we can rewrite $\boldsymbol{E}_{ik}$ as

$$\boldsymbol{E}_{ik} = S_i\|\boldsymbol{v}_i\|^2 D_{ik}\frac{\boldsymbol{v}_i\boldsymbol{v}_i^T}{\|\boldsymbol{v}_i\|^2} + S_{e_i}\boldsymbol{I} = \bar{S}_i D_{ik}\overline{\boldsymbol{v}}_i\overline{\boldsymbol{v}}_i^T + S_{e_i}\boldsymbol{I} \tag{9}$$

where $\overline{\boldsymbol{v}}_i = \|\boldsymbol{v}_i\|^{-1}\boldsymbol{v}_i$ is the local mode shape with unit norm, and

$$\bar{S}_i = S_i\|\boldsymbol{v}_i\|^2 \tag{10}$$

is now the modal force PSD 'scaled locally', i.e., corresponding to the local mode shape scaled to have unit norm. It should be distinguished from S_i which is 'scaled globally', i.e., corresponding to the global mode shape $\boldsymbol{\varphi}$ scaled to have unit norm. In terms of $\bar{S}_i$ and $\overline{\boldsymbol{v}}_i$ (instead of S_i and $\boldsymbol{v}_i$), $\boldsymbol{E}_{ik}$ has the same form as in the single setup situation and so we can use previous results [28] to predict the behavior of $\partial^2 L_i/\partial\theta^2$. Let $\boldsymbol{\theta}_i = \{\boldsymbol{\varpi}_i, \boldsymbol{v}_i\} = \{f_i, \zeta_i, \bar{S}_i, S_{e_i}, \boldsymbol{v}_i\}$ denote the parameters in Setup i and $\boldsymbol{\varpi}_i = \{f_i, \zeta_i, \bar{S}_i, S_{e_i}\}$ excludes the mode shape. Then asymptotically

$$\frac{\partial^2 L_i}{\partial \theta_i^2} = \begin{bmatrix} \frac{\partial^2 L_i}{\partial \varpi_i^2} & \\ & \frac{\partial^2 L_i}{\partial v_i^2} \end{bmatrix} \qquad \frac{\partial^2 L_i}{\partial v_i^2} = k_i\left(\boldsymbol{I} - \overline{\boldsymbol{v}}_i \overline{\boldsymbol{v}}_i^T\right) \tag{11}$$

where k_i was defined in (7). The expression of $\partial^2 L/\partial v_i^2$ is the same as the one previously found for single setup data except that the modal force PSD in the definition of k_i is now the one scaled globally rather than locally.

4.1 Decorrelation between parameters

To facilitate analysis, let the total set of parameters be arranged as $\boldsymbol{\theta} = \{\boldsymbol{\varpi}_1, \dots, \boldsymbol{\varpi}_{n_s}, \boldsymbol{\varphi}\}$. Recalling $\boldsymbol{v}_i = \boldsymbol{L}_i \boldsymbol{\varphi}$ and assembling the partitions in (11) into $\partial^2 L/\theta^2$ gives

$$\frac{\partial^2 L}{\partial \theta^2} = \begin{bmatrix} \frac{\partial^2 L_1}{\partial \varpi_1^2} & & & \\ & \ddots & & \\ & & \frac{\partial^2 L_{n_s}}{\partial \varpi_{n_s}^2} & \\ & & & \boldsymbol{J} \end{bmatrix} \tag{12}$$

where

$$\boldsymbol{J} = \frac{\partial^2 L}{\partial \varphi^2} = \sum_i \boldsymbol{L}_i^T \frac{\partial^2 L_i}{\partial v_i^2} \boldsymbol{L}_i \tag{13}$$

The multiplicative terms in $\boldsymbol{J}$ related to $\boldsymbol{L}_i$ stems from the chain rule $\partial(\cdot)/\partial \boldsymbol{\varphi} = [\partial(\cdot)/\partial \boldsymbol{v}_i][\partial \boldsymbol{v}_i/\partial \boldsymbol{\varphi}] = [\partial(\cdot)/\partial \boldsymbol{v}_i]\boldsymbol{L}_i$. In (12), the cross-partitions between $\boldsymbol{\varpi}_i$ and $\boldsymbol{\varpi}_j$ ($i \neq j$) are zero because L_i does not depend on $\boldsymbol{\varpi}_j$; and this implies that the parameters (except mode shape) in different setups are asymptotically uncorrelated. On the other hand, the cross-partitions between the $\boldsymbol{\varpi}_i$s and $\boldsymbol{\varphi}$ are zero because $\boldsymbol{\varpi}_i$ does not depend on $\boldsymbol{v}_j$ ($i \neq j$) and it is asymptotically uncorrelated from $\boldsymbol{v}_i$, as seen in (11); and this implies that in a multiple setup situation the mode shape is also uncorrelated from the remaining parameters. Since the inverse of a block diagonal matrix is equal to a block diagonal matrix of the individual inverses, the covariance matrix of each $\boldsymbol{\varpi}_i = \{f_i, \zeta_i, \bar{S}_i, S_{e_i}\}$ is simply equal to the inverse of $\partial^2 L_i/\partial \varpi_i^2$, i.e., their single setup counterpart. Similarly, the covariance matrix of $\boldsymbol{\varphi}$ is equal to the (pseudo) inverse of $\boldsymbol{J}$ in (13). Substituting $\partial^2 L/\partial v_i^2$ in (11) into (13) gives (6).

Although the results here are based on a parameterization with $\bar{S}_i$, they also apply to $S_i = \|\boldsymbol{v}_i\|^{-2}\bar{S}_i = \left(\boldsymbol{v}_i^T\boldsymbol{v}_i\right)^{-1}\bar{S}_i$. To see this, note that their uncertain perturbations (denoted by Δ) are related by

$$\Delta S_i = \left(\boldsymbol{v}_i^T\boldsymbol{v}_i\right)^{-1}\Delta\bar{S}_i - 2\left(\boldsymbol{v}_i^T\boldsymbol{v}_i\right)^{-2}\Delta\boldsymbol{v}_i^T\boldsymbol{v}_i\bar{S}_i \tag{14}$$

The correlation of the first term with $\Delta\boldsymbol{v}_i$ is of the same order as the correlation between $\Delta\bar{S}_i$ and $\Delta\boldsymbol{v}_i$, which is asymptotically small (as just established). The covariance of the second term with $\Delta\boldsymbol{v}_i$ is $-2\left(\boldsymbol{v}_i^T\boldsymbol{v}_i\right)^{-2}E\left[\Delta\boldsymbol{v}_i\Delta\boldsymbol{v}_i^T\right]\boldsymbol{v}_i\bar{S}_i$. Since $E[\Delta S_i^2]$ and $E[\Delta\boldsymbol{v}_i\Delta\boldsymbol{v}_i^T]$ are respectively $O(S_i^2)$ and $O(k_i^{-1})$ [28], the correlation between S_i and $\boldsymbol{v}_i$ will be $O\left(k_i^{-1/2}\right)$, which is asymptotically small and hence the claim follows.

4.2 Fixed reference DOFs and distinct rover DOFs

To gain further insights on mode shape uncertainty beyond (6), we now narrow the scope to the case of fixed reference DOFs and distinct rover DOFs in different setups. An additional technical assumption is that in any given setup a DOF is measured by at most one data channel. In this case, let the global mode shape be partitioned as

$$\boldsymbol{\varphi} = \begin{bmatrix}\boldsymbol{u}_R\\ \boldsymbol{u}_1\\ \vdots\\ \boldsymbol{u}_{n_s}\end{bmatrix} \tag{15}$$

where $\boldsymbol{u}_R$ $(n_R \times 1)$ corresponds to the partial mode shape of the reference DOFs; $\boldsymbol{u}_i$ $(n_{vi} \times 1)$ corresponds to the partial mode shape of the rover DOFs of the ith setup, $i = 1, \dots, n_s$. Since the reference DOFs are assumed to be fixed, the DOFs covered by $\boldsymbol{v}_i$ comprise those from $\boldsymbol{u}_R$ and $\boldsymbol{u}_i$. The local mode shape $\boldsymbol{v}_i$ and $[\boldsymbol{u}_R; \boldsymbol{u}_i]$ are related by a permutation matrix (omitted here) that accounts for the data channel ordering in Setup i. Corresponding to (15), $\boldsymbol{J}$ has the partitioned form

$$\boldsymbol{J} = \begin{bmatrix}\boldsymbol{J}_{RR} & \boldsymbol{J}_{R1} & \cdots & \boldsymbol{J}_{Rn_s}\\ \boldsymbol{J}_{1R} & \boldsymbol{J}_{11} & & \\ \vdots & & \ddots & \\ \boldsymbol{J}_{n_sR} & & & \boldsymbol{J}_{n_sn_s}\end{bmatrix} \tag{16}$$

where $\boldsymbol{J}_{iR} = \boldsymbol{J}_{Ri}^T$ because Hessian matrix is symmetric. The cross-partitions $\boldsymbol{J}_{ij}$ ($i \neq j$) between the rover DOFs in different setups are zero because the setups do not share any common rover DOFs.

As an outline, in Sections 4.3 to 4.7 we first derive using (16) the eigenvalue properties of $\boldsymbol{J}$ as reported in Table 1. Since the eigenvectors of $\boldsymbol{J}$ (real-symmetric) are orthogonal, one can then write $\boldsymbol{J}$ as the sum of contributions from different eigenspaces:

$$\boldsymbol{J} = \boldsymbol{J}_R + \boldsymbol{J}_V + \boldsymbol{J}_G \tag{17}$$

where the contribution from each type (indicated by subscript) is a sum $\Sigma_i \lambda_i \boldsymbol{x}_i \boldsymbol{x}_i^T$ over all eigenvalues of the type; λ_i and $\boldsymbol{x}_i$ denote respectively an eigenvalue and the corresponding eigenvector. The pseudo-inverse (ignoring type N) of $\boldsymbol{J}$ is given by the sum of individual inverses:

$$\boldsymbol{J}^+ = \boldsymbol{J}_R^{-1} + \boldsymbol{J}_V^{-1} + \boldsymbol{J}_G^{-1} \tag{18}$$

where the contribution from each type is a sum $\Sigma_i \lambda_i^{-1} \boldsymbol{x}_i \boldsymbol{x}_i^T$ with the eigenvalues replaced by their reciprocals. The eigenvalues of type R and V are explicitly known and hence their reciprocals that contribute to the global mode shape c.o.v. can be obtained. Analytical solution for type G eigenvalues has not been found but it turns out that the sum of their reciprocals can be obtained in a manageable form, giving the contribution δ_G^2 to global mode shape c.o.v. (squared) as summarized in Table 2. The bounds on δ_G^2 in (8) are derived in Section 4.8. The lower bound is reasoned from first principle. The upper bound is derived by analyzing δ_G^2 as a quadratic function of $\{c_i\}_{i=1}^{n_s}$ subjected to mode shape norm constraint.

4.3 Eigenvalue equation in partitioned form

The basic approach adopted to solve the eigenvalue problem $\boldsymbol{J}\boldsymbol{x} = \lambda \boldsymbol{x}$ is to consider a candidate form of the eigenvector $\boldsymbol{x}$ (guess by observation) and then substitute it into the equation to determine the eigenvalue and unknown coefficients (if any). The validity of the form of eigenvector is verified automatically when the equations are satisfied.

Consistent with (15), let an eigenvector of $\boldsymbol{J}$ be partitioned as

$$\boldsymbol{x} = \begin{bmatrix} \boldsymbol{x}_R \\ \boldsymbol{x}_1 \\ \vdots \\ \boldsymbol{x}_{n_s} \end{bmatrix} \tag{19}$$

Substituting (16) and (19) into $\boldsymbol{J}\boldsymbol{x} = \lambda \boldsymbol{x}$ and multiplying the partitions gives the following system of matrix equations that is equivalent to the original eigenvalue equation:

$$\boldsymbol{J}_{RR}\boldsymbol{x}_R + \Sigma_i \boldsymbol{J}_{Ri}\boldsymbol{x}_i = \lambda \boldsymbol{x}_R \tag{20}$$

$$\boldsymbol{J}_{iR}\boldsymbol{x}_R + \boldsymbol{J}_{ii}\boldsymbol{x}_i = \lambda \boldsymbol{x}_i \qquad (i = 1, \dots, n_s) \tag{21}$$

In Sections 4.4 to 4.7 to follow, we will consider different candidate forms of $\boldsymbol{x}$ in terms of its partitions, which will lead to different types of eigenvectors. To facilitate the analysis of (20) and (21), the partitions are expressed in terms of the local mode shapes:

$$\boldsymbol{J}_{RR} = \Sigma_j k_j \left(\boldsymbol{I} - b_j^{-1}\boldsymbol{u}_R\boldsymbol{u}_R^T\right) \tag{22}$$

$$\boldsymbol{J}_{ii} = k_i \left(\boldsymbol{I} - b_i^{-1}\boldsymbol{u}_i\boldsymbol{u}_i^T\right) \tag{23}$$

$$\boldsymbol{J}_{Ri} = -k_i b_i^{-1}\boldsymbol{u}_R\boldsymbol{u}_i^T \tag{24}$$

where k_i was defined in (7) and

$$b_i = \|\boldsymbol{v}_i\|^2 \tag{25}$$

is defined for convenience. See Appendix A for the derivation of (22) to (24).

4.4 Type N (mode shape norm constraint)

As a consequence of mode shape norm constraint, $\boldsymbol{J}$ has a zero eigenvalue with eigenvector $\boldsymbol{\varphi}$. This can be easily checked by substituting $\boldsymbol{x} = \boldsymbol{\varphi} = \left[\boldsymbol{u}_R; \boldsymbol{u}_1; \cdots; \boldsymbol{u}_{n_s}\right]$ into (20) and (21). In particular, for (20),

$$\boldsymbol{J}_{RR}\boldsymbol{u}_R = \Sigma_j k_j \left(\boldsymbol{I} - b_j^{-1}\boldsymbol{u}_R\boldsymbol{u}_R^T\right)\boldsymbol{u}_R = \Sigma_j k_j \left(1 - \frac{c_R}{b_j}\right)\boldsymbol{u}_R = \Sigma_j k_j \frac{c_j}{b_j}\boldsymbol{u}_R \tag{26}$$

$$\boldsymbol{J}_{Ri}\boldsymbol{u}_i = -k_i b_i^{-1}\boldsymbol{u}_R\boldsymbol{u}_i^T\boldsymbol{u}_i = -k_i \frac{c_i}{b_i}\boldsymbol{u}_R \tag{27}$$

where

$$c_R = \|\boldsymbol{u}_R\|^2 \qquad c_i = \|\boldsymbol{u}_i\|^2 \qquad c_R + c_i = b_i \tag{28}$$

The LHS of (20) with $\boldsymbol{x} = \left[\boldsymbol{u}_R; \boldsymbol{u}_1; \cdots; \boldsymbol{u}_{n_s}\right]$ then reads

$$\boldsymbol{J}_{RR}\boldsymbol{u}_R + \Sigma_i \boldsymbol{J}_{Ri}\boldsymbol{u}_i = \Sigma_i \left(k_j \frac{c_j}{b_j} - k_j \frac{c_j}{b_j}\right)\boldsymbol{u}_R = 0 \cdot \boldsymbol{u}_R \tag{29}$$

For (21),

$$\boldsymbol{J}_{iR}\boldsymbol{u}_R = -k_i b_i^{-1}\boldsymbol{u}_i \boldsymbol{u}_R^T \boldsymbol{u}_R = -k_i \frac{c_R}{b_i}\boldsymbol{u}_i \tag{30}$$

$$\boldsymbol{J}_{ii}\boldsymbol{u}_i = k_i\left(\boldsymbol{I} - b_i^{-1}\boldsymbol{u}_i\boldsymbol{u}_i^T\right)\boldsymbol{u}_i = k_i\left(1 - \frac{c_i}{b_i}\right)\boldsymbol{u}_i = k_i \frac{c_R}{b_i}\boldsymbol{u}_i \tag{31}$$

The LHS of (21) then reads

$$\boldsymbol{J}_{iR}\boldsymbol{u}_R + \boldsymbol{J}_{ii}\boldsymbol{u}_i = \left(-k_i \frac{c_R}{c_i} + k_i \frac{c_R}{b_i}\right)\boldsymbol{u}_i = 0 \cdot \boldsymbol{u}_i \tag{32}$$

Equations (29) and (32) imply that that $\boldsymbol{x} = \left[\boldsymbol{u}_R; \boldsymbol{u}_1; \cdots; \boldsymbol{u}_{n_s}\right]$ is indeed an eigenvector of $\boldsymbol{J}$ with eigenvalue 0, as reported in Table 1.

4.5 Type R (Local uncertainty confined to reference DOFs)

Consider eigenvector of the form $\boldsymbol{x} = [\boldsymbol{u}_R'; \boldsymbol{0}; \cdots; \boldsymbol{0}]$ where $\boldsymbol{u}_R'$ $(n_R \times 1)$ is orthogonal to $\boldsymbol{u}_R$, i.e., $\boldsymbol{u}_R^T\boldsymbol{u}_R' = 0$. The LHS of (20) and (21) then read, respectively,

$$\boldsymbol{J}_{RR}\boldsymbol{u}_R' + \Sigma_i \boldsymbol{J}_{Ri} \cdot \boldsymbol{0} = \Sigma_i k_i\left(\boldsymbol{u}_R' - b_i^{-1}\boldsymbol{u}_R\boldsymbol{u}_R^T\boldsymbol{u}_R'\right) = (\Sigma_i k_i)\boldsymbol{u}_R' \tag{33}$$

$$\boldsymbol{J}_{iR}\boldsymbol{u}_R' + \boldsymbol{J}_{ii} \cdot \boldsymbol{0} = -k_i b_i^{-1}\boldsymbol{u}_i\boldsymbol{u}_R^T\boldsymbol{u}_R' = \boldsymbol{0} \tag{34}$$

The above implies that $\boldsymbol{x} = [\boldsymbol{u}_R'; \boldsymbol{0}; \cdots; \boldsymbol{0}]$ is indeed an eigenvector and the eigenvalue is $\Sigma_i k_i$, as reported in Table 1. Since the orthogonal complement of $\boldsymbol{u}_R$ has a dimension of $(n_R - 1)$, there are $(n_R - 1)$ possible eigenvectors of this type. They must be mutually orthogonal in order that their corresponding eigenvectors of the form $\boldsymbol{x} = [\boldsymbol{u}_R'; \boldsymbol{0}; \cdots; \boldsymbol{0}]$ are mutually orthogonal, because $\boldsymbol{J}$ is real and symmetric. Summing the reciprocals of the $(n_R - 1)$ eigenvalues gives the contribution of global mode shape c.o.v. from type R in Table 2.

4.6 Type V (Local uncertainty confined to rover DOFs)

Similar to type R, consider a candidate eigenvector where only the partition of the rover DOFs in Setup i is non-zero and is equal to $\boldsymbol{u}_i'$. Here, $\boldsymbol{u}_i'$ $(n_{vi} \times 1)$ is orthogonal to $\boldsymbol{u}_i$, i.e., $\boldsymbol{u}_i^T \boldsymbol{u}_i' = 0$. The LHS of (20) and (21) then read, respectively,

$$\boldsymbol{J}_{RR} \cdot \boldsymbol{0} + \Sigma_j \boldsymbol{J}_{Rj} \boldsymbol{u}_j' = -k_i b_i^{-1} \boldsymbol{u}_R \boldsymbol{u}_i^T \boldsymbol{u}_i' = k_i \cdot \boldsymbol{0} \tag{35}$$

$$\boldsymbol{J}_{iR} \cdot \boldsymbol{0} + \boldsymbol{J}_{ii} \boldsymbol{u}_i' = k_i \left(\boldsymbol{I} - b_i^{-1} \boldsymbol{u}_i \boldsymbol{u}_i^T \right) \boldsymbol{u}_i' = k_i \left(\boldsymbol{u}_i' - b_i^{-1} \boldsymbol{u}_i \boldsymbol{u}_i^T \boldsymbol{u}_i' \right) = k_i \boldsymbol{u}_i' \tag{36}$$

The above shows that the candidate vector is indeed an eigenvector with eigenvalue k_i, as reported in Table 1. For each Setup i, since the orthogonal complement of $\boldsymbol{u}_i$ has dimension $(n_{vi} - 1)$, there are $(n_{vi} - 1)$ possible eigenvectors of this type. They must be mutually orthogonal in order that their corresponding eigenvectors of $\boldsymbol{J}$ are orthogonal. Summing the reciprocals of the $(n_{vi} - 1)$ eigenvalues of Setup i and over all setups $(i = 1, \dots, n_s)$ gives the contribution of global mode shape c.o.v. from type R in Table 2.

4.7 Type G (Global uncertainty, involving all DOFs)

The eigenvectors of type R and V considered in the last two sections are 'local' in the sense that their non-zero values are confined respectively to the reference DOFs and rover DOFs of a particular setup, while the values at other DOFs are zero. Within the local DOFs the eigenvector is orthogonal to the mode shape, which is the same as the one for a single setup. In addition to these local types, there are non-trivial eigenvectors of 'global' nature that involve all the DOFs. Consider a candidate eigenvector of the form

$$\boldsymbol{x} = \begin{bmatrix} a_R \boldsymbol{u}_R \\ a_1 \boldsymbol{u}_1 \\ \vdots \\ a_{n_s} \boldsymbol{u}_{n_s} \end{bmatrix} = \begin{bmatrix} \boldsymbol{u}_R & & & \\ & \boldsymbol{u}_1 & & \\ & & \ddots & \\ & & & \boldsymbol{u}_{n_s} \end{bmatrix} \begin{bmatrix} a_R \\ a_1 \\ \vdots \\ a_{n_s} \end{bmatrix} = \boldsymbol{U}\boldsymbol{a} \tag{37}$$

where a_R and a_i $(i = 1, \dots, n_s)$ are scalar coefficients. That is, within each partition the eigenvector is proportional to the mode shape, but the coefficients associated with different partitions are not necessarily equal to 1. Substituting $\boldsymbol{x} = \boldsymbol{U}\boldsymbol{a}$ into $\boldsymbol{J}\boldsymbol{x} = \lambda \boldsymbol{x}$ and pre-multiplying both sides by $\boldsymbol{U}^T$ gives the generalized eigenvalue problem $\boldsymbol{D}\boldsymbol{a} = \lambda \boldsymbol{C}\boldsymbol{a}$, where

$$\boldsymbol{D} = \boldsymbol{U}^T\boldsymbol{J}\boldsymbol{U} = \begin{bmatrix} \Sigma_i d_i & -d_1 & \cdots & -d_{n_s} \\ -d_1 & d_1 & & \\ \vdots & & \ddots & \\ -d_{n_s} & & & d_{n_s} \end{bmatrix} \qquad \boldsymbol{C} = \boldsymbol{U}^T\boldsymbol{U} = \begin{bmatrix} c_R & & & \\ & c_1 & & \\ & & \ddots & \\ & & & c_{n_s} \end{bmatrix} \tag{38}$$

are real-symmetric matrices; $c_R = \|\boldsymbol{u}_R\|^2$ and $c_i = \|\boldsymbol{u}_i\|^2$ were defined in (28); and

$$d_i = \frac{k_i c_i}{b_i} c_R \tag{39}$$

The entries in (38) can be derived with the help of (26), (27), (30) and (31). Note that each row of $\boldsymbol{D}$ sums to zero. It then follows that $\boldsymbol{a} = [1, \dots, 1]^T$ is an eigenvector with eigenvalue 0, which corresponds to the type N eigenvector $\boldsymbol{x} = \boldsymbol{\varphi}$ found earlier in Section 4.4. The remaining n_s eigenvalues are all non-negative (as expected). To see this, for any $(n_s + 1) \times 1$ vector $\boldsymbol{a}$ we have $\boldsymbol{a}^T\boldsymbol{D}\boldsymbol{a} = (\boldsymbol{U}\boldsymbol{a})^T\boldsymbol{J}(\boldsymbol{U}\boldsymbol{a}) \geq 0$ since $\boldsymbol{J}$ is positive semi-definite. As eigenvectors $\boldsymbol{a}$ of the generalised eigenvalue problem are orthogonal with respect to $\boldsymbol{C} = \boldsymbol{U}^T\boldsymbol{U}$, the corresponding $\boldsymbol{x} = \boldsymbol{U}\boldsymbol{a}$ are orthogonal, consistent with the real-symmetric nature of $\boldsymbol{J}$.

Manageable analytical solution for $\boldsymbol{D}\boldsymbol{a} = \lambda\boldsymbol{C}\boldsymbol{a}$ has not been found but it is still possible to obtain the sum of reciprocals of the eigenvalues that gives the type G contribution δ_G^2 to mode shape c.o.v. (squared). For this purpose, we first eliminate a_R from the problem as follows. The first and subsequent ith row of partition of $\boldsymbol{D}\boldsymbol{a} = \lambda\boldsymbol{C}\boldsymbol{a}$ reads

$$\begin{matrix} \sum_i d_i(a_R - a_i) = \lambda c_R a_R \\ -d_i(a_R - a_i) = \lambda c_i a_i \end{matrix} \qquad i = 1, \dots, n_s \tag{40}$$

If $\lambda = 0$ the only solution to (40) is $a_R = a_i$ $(i = 1, \dots, n_s)$, which corresponds to type N eigenvector. Now consider $\lambda \neq 0$. Substituting the second equation into the summand of the first and rearranging gives $a_R = -\Sigma_i a_i c_i / c_R$. This implies (as expected) that the corresponding eigenvector $\boldsymbol{x} = \boldsymbol{U}\boldsymbol{a}$ is orthogonal to $\boldsymbol{\varphi}$, because $\boldsymbol{x}^T\boldsymbol{\varphi} = a_R c_R + \Sigma_i a_i c_i = 0$. Substituting $a_R = -\Sigma_i a_i c_i / c_R$ into the equations for $i = 1, \dots, n_s$ in (40) gives the standard eigenvalue problem $\boldsymbol{D}_c\boldsymbol{a}_c = \lambda\boldsymbol{a}_c$ where $\boldsymbol{a}_c = \left[a_1, \dots, a_{n_s}\right]^T$ excludes a_R and the entries of $\boldsymbol{D}_c$ $(n_s \times n_s)$ are given by

$$\boldsymbol{D}_c(i,i) = k_i \qquad \boldsymbol{D}_c(i,j) = k_i \frac{c_j}{b_i} \qquad i, j = 1, \dots, n_s; j \neq i \tag{41}$$

Similar to $\boldsymbol{Da} = \lambda \boldsymbol{Ca}$, manageable analytical solution for $\boldsymbol{D}_c \boldsymbol{a}_c = \lambda \boldsymbol{a}_c$ has not been found. However, it is found that the inverse of $\boldsymbol{D}_c$ has a simple form:

$$\boldsymbol{D}_c^{-1}(i,i) = \frac{b_i(1-c_i)}{k_i c_R} \qquad \boldsymbol{D}_c^{-1}(i,j) = -\frac{b_j c_j}{k_j c_R} \qquad i,j = 1,\dots,n_s; j \neq i \tag{42}$$

Summing the diagonal entries of $\boldsymbol{D}_c^{-1}$, substituting $b_i = c_R + c_i$ from (28) and simplifying gives the expression of δ_G^2 in Table 2. As a remark, theoretically one can obtain the eigenvectors of $\boldsymbol{a} = \left[a_R, a_1, \dots, a_{n_s}\right]^T$ by either solving $\boldsymbol{Da} = \lambda \boldsymbol{Ca}$ or $\boldsymbol{D}_c \boldsymbol{a}_c = \lambda \boldsymbol{a}_c$. Computationally, however, the former is recommended (as in Table 1) because standard algorithms dealing with real symmetric matrices have better numerical properties.

4.8 Bounds on mode shape uncertainty

The partial mode shape norms $c_i = \|\boldsymbol{u}_i\|^2, i = 1,\dots,n_s$, are the only parameters related to how the rovers are planned. Consider fixing the reference DOFs, hence $c_R = \|\boldsymbol{u}_R\|^2$, and study how the global mode shape c.o.v. δ^2 depends on $\{c_i\}_{i=1}^{n_s}$. This should be subjected to the global mode shape norm constraint $c_R + \Sigma_i c_i = 1$. From Table 2, among the different types of contributions, only type G depends on $\{c_i\}_{i=1}^{n_s}$ and so it is sufficient to study how δ_G^2 depends on $\{c_i\}_{i=1}^{n_s}$ subjected to $c_R + \Sigma_i c_i = 1$. The lower bound of δ_G^2 in (8) has been reasoned in Section 3.3.1 and so it remains to derive the upper bound. For this purpose, rewrite δ_G^2 in Table 2 as a quadratic form:

$$\delta_G^2 = \Sigma_i k_i^{-1} + \frac{1}{2c_R} \boldsymbol{c}^T \boldsymbol{A} \boldsymbol{c} \tag{43}$$

where $\boldsymbol{c} = \left[c_1, \dots, c_{n_s}\right]^T$ and $\boldsymbol{A}$ is a $n_s \times n_s$ matrix whose entries are given by

$$\boldsymbol{A}(i,i) = 0 \qquad \boldsymbol{A}(i,j) = k_i^{-1} + k_j^{-1} \qquad i,j = 1,\dots,n_s; i \neq j \tag{44}$$

Now consider the following Lagrangian that incorporates the constraint $c_R + \Sigma_i c_i = 1$:

$$F(\boldsymbol{c}) = \delta_G^2 + \mu(1 - c_R - \Sigma_i c_i) = \Sigma_i k_i^{-1} + \frac{1}{2c_R} \boldsymbol{c}^T \boldsymbol{A} \boldsymbol{c} + \mu(1 - c_R - \boldsymbol{1}^T \boldsymbol{c}) \tag{45}$$

where μ is a Lagrange multiplier and $\boldsymbol{1} = [1,\dots,1]^T$ denotes a vector of ones. Solving $\partial F / \partial \boldsymbol{c} = \boldsymbol{0}$ for $\boldsymbol{c}$ together with the constraint gives

$$\hat{\mu} = \frac{1-c_R}{c_R Q} \qquad \hat{\boldsymbol{c}} = \frac{1-c_R}{Q}\boldsymbol{A}^{-1}\mathbf{1} \qquad Q = \mathbf{1}^T\boldsymbol{A}^{-1}\mathbf{1} = \Sigma_{i,j}\boldsymbol{A}^{-1}(i,j) \tag{46}$$

Substituting $\boldsymbol{c} = \hat{\boldsymbol{c}}$ into (43) and simplifying gives the rightmost expression in (8). It is shown in Appendix B that the Hessian of δ_G^2 with respect to $\boldsymbol{c}$ satisfying the constraint is a negative semi-definite constant matrix, and so $\hat{\boldsymbol{c}}$ corresponds to the global maximum of δ_G^2, i.e., an upper bound. Since the inequality constraints $0 \leq \hat{c}_i \leq 1 - c_R$ $(i = 1, \dots, n_s)$ have not been explicitly imposed in the above analysis, it is possible that $\hat{\boldsymbol{c}}$ does not lie in the admissible region. If it does, the global maximum can be achieved, in which case the upper bound is the tightest possible one.

5 Verification with synthetic data

In this section, synthetic data is used to validate the uncertainty law with multiple setup data. Consider an eleven-storied shear building with uniform floor mass and story stiffness of 500 tons and 1000 kN/mm, respectively. The natural frequencies of the first four modes are calculated to be 0.97 Hz, 2.9 Hz, 4.77 Hz, and 6.55 Hz. Assume classically damped modes with damping ratios of 1% for all modes. The structure is subjected to horizontal independent and identically distributed (i.i.d.) Gaussian white noise excitation with a PSD of 24.06 N^2/Hz per floor. Figure 1(a) shows the setup that covers the 11 horizontal DOFs in three setups. The top two levels are chosen as reference DOFs. The remaining levels will be covered by rover DOFs. Theoretical modal force PSDs (scaled globally) of the first mode for the three setups are calculated to be $S_1 = 0.75$ (μg)^2/Hz , $S_2 = 0.55$ (μg)^2/Hz and $S_3 = 0.38$ (μg)^2/Hz. Acceleration data is generated at a sampling rate of 100 Hz. It is contaminated by i.i.d. Gaussian white noise with a PSD of 10 (μg)^2/Hz. Based on $\gamma_i = S_i\|\boldsymbol{v}_i\|^2/4S_{e_i}\zeta_i^2$ in (4), the theoretical modal s/n ratio of the first mode in the three setups are $\gamma_1 = 186.85$, $\gamma_2 = 137.23$, and $\gamma_3 = 95.83$. Figure 1(b) shows the root singular value (SV) spectrum based on 300 seconds of data in Setup 1. The BAYOMA algorithm for well-separated modes incorporating multiple setup data is used for calculating the posterior MPV [26] and covariance matrix [27] of modal parameters for given data. This applies to the BAYOMA results in Section 6 as well. The frequency band and initial guess of frequency used in the algorithm are indicated in Figure 1(b) by horizontal bar below the spectral peaks and a circle, respectively.

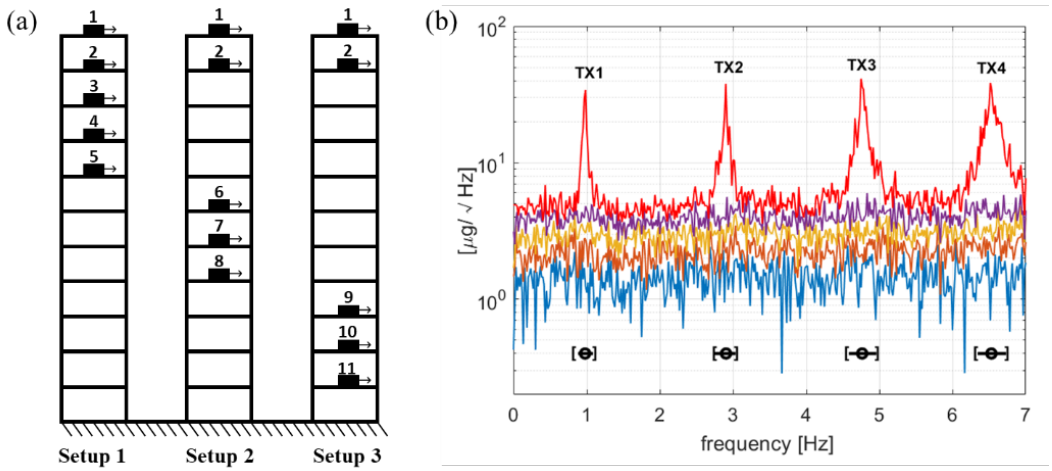

Figure 1. (a) Setup plan; (b) Root SV spectrum in Setup 1.

5.1 Principal mode shape uncertainty

We first investigate the eigenvector properties of the posterior covariance matrix of the global mode shape, which give the (mutually uncorrelated) principal directions where uncertainty can take place. Recall the prediction from uncertainty law in Table 1. In this example, there are $n_R = 2$ reference DOFs, giving $(n_R - 1) = 1$ eigenvector of type R, i.e., with non-zero value in the reference DOFs only. For type V, each setup ($i = 1,2,3$) has $n_{vi} = 3$ rover DOFs and hence $(n_{vi} - 1) = 2$ eigenvectors with non-zero value in the rover DOFs of the setup only. Type G has $n_s = 3$ eigenvectors, with non-zero values in all measured DOFs.

The above predictions from uncertainty law are verified in Figure 2, which shows the eigenvectors of the 11×11 global mode shape posterior covariance matrix of Mode 1 from BAYOMA algorithm with 300 seconds of data in each setup. The type and eigenvalue are also indicated. The eigenvector of type N (top left corner) is simply the MPV of global mode shape. The eigenvectors in the bottom row (type R and V) are all local in nature. Here, V2 denotes type V localized to Setup 2, for which the eigenvectors are plotted together in different colors and line types. The eigenvectors in the top row (G1, G2, G3) are global in nature, involving all DOFs. Consistent with the prediction by uncertainty law, the local shapes within the reference DOFs or rover DOFs in a particular setup are similar to the counterparts of the mode shape. Nevertheless, the overall spatial pattern that involves scaling of different parts is non-trivial.

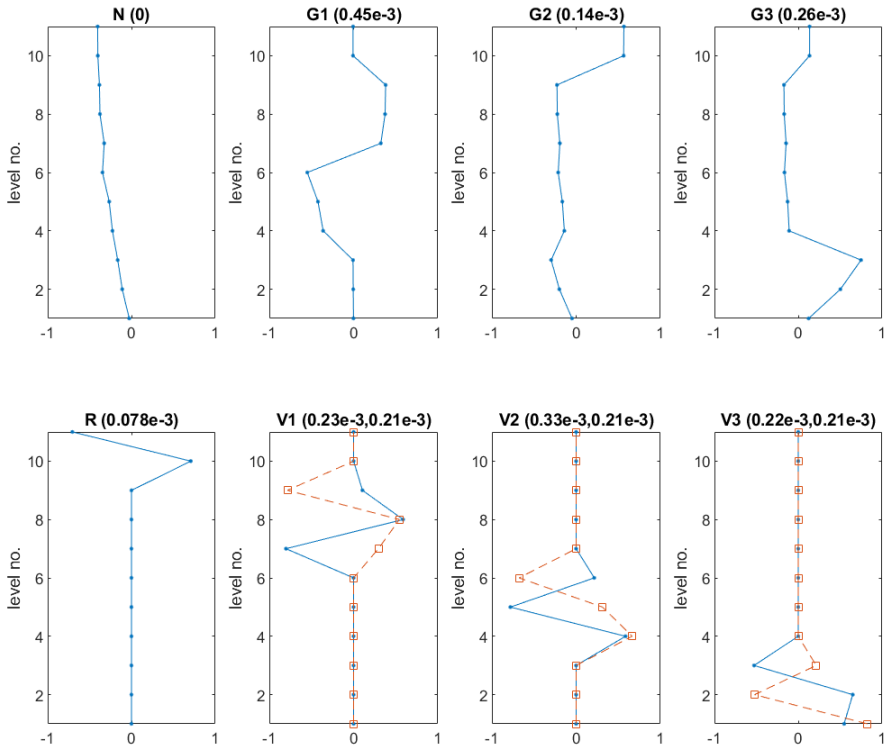

Figure 2 Principal directions (eigenvectors) of global mode shape uncertainty. Value in parenthesis indicates the eigenvalue. Type 'N' for 'norm constraint'; 'R' involves reference DOFs only; 'V' (followed by setup number) involves rover DOFs only, eigenvectors are distinguished by blue-dot-solid line and red-square-dash line; 'G' involves all DOFs.

5.2 Data length effect

We next investigate how the ID uncertainty depends on data length. Figure 3 shows the posterior c.o.v.s of the modal parameters of Mode 1 in Setup 1 versus the normalized data length N_c (i.e., as a multiple of natural period). For each modal parameter, the black stars and red squares show the values from BAYOMA algorithm (for given data) and uncertainty law, respectively. For the latter, the parameters in the formula are substituted by their MPVs for the given data, as is often done. The two sets of values (stars and squares) generally agree and converge to each other as data length increases, verifying the mathematical correctness of the uncertainty law. The results for other modes and setups (omitted here) are qualitatively similar.

Figure 4 shows the global mode shape c.o.v. versus the normalized data length. The values from BAYOMA algorithm (given data) and uncertainty law are shown with stars and squares, respectively. In addition to the 'total' c.o.v. δ (black), the c.o.v. of different types, i.e., δ_R (red), δ_V (blue) and δ_G (green) are also shown. It is seen that the uncertainty law values capture well

the BAYOMA values, demonstrating mathematical correctness of the theory. The contribution from type R is smallest, which is reasonable because reference DOFs are measured repeatedly in different setups. Type V gives the major contribution to mode shape c.o.v., attributed in part to their abundance in number. For example, Figure 2 shows that the eigenvalues (shown in parenthesis) of type G and type V eigenvector are of similar order of magnitude; and some type G eigenvalue can be greater than type V.

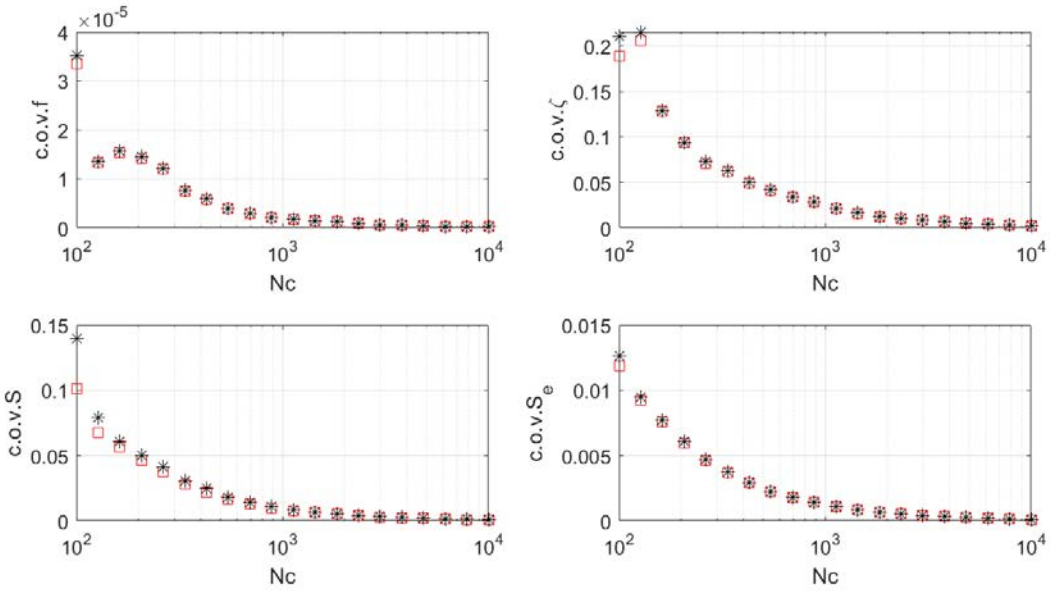

Figure 3. Posterior c.o.v. of modal parameters vs N_c = data length/natural period. Mode 1, Setup 1, synthetic data; stars for values from BAYOMA algorithm (given data) and squares for uncertainty law.

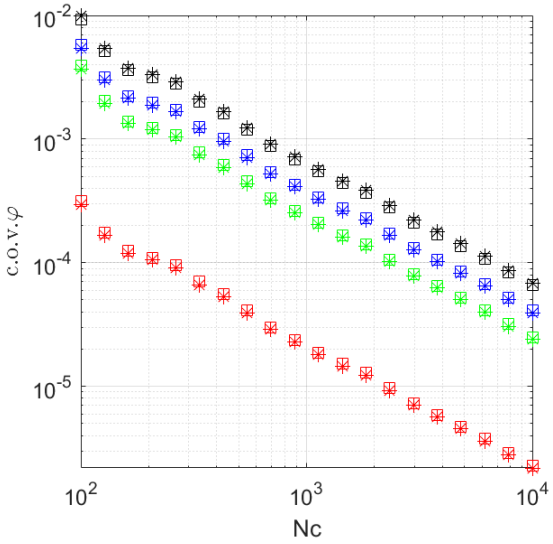

Figure 4. Posterior c.o.v. of global mode shape vs N_c = data length/natural period. Mode 1, synthetic data; stars for values from BAYOMA algorithm (given data), squares for uncertainty law; Black for total c.o.v. (δ), red for R (δ_R), blue for V (δ_V), green for G (δ_G).

5.3 Modal s/n ratio effect

The effect of modal s/n ratio is next investigated. The focus is on the global mode shape, since the effect on the remaining parameters is the same as in a single setup setting that has been studied previously [29]. Table 2 reveals that the c.o.v. of global mode shape depends on the modal s/n ratios of different setups in a non-trival aggregate manner. Consider a data duration of 2,000 seconds in each setup, which corresponds to $N_c = 1{,}940$ for the first mode. As the focus is on modal s/n ratio, a relatively long duration is considered here to reduce spurious data length effects. Modal identification results are obtained from BAYOMA algorithm for 100 data sets. They are contaminated with noise PSD ranging logarithmically from 250 $(\mu g)^2$/Hz to 0.25 $(\mu g)^2$/Hz, corresponding to a modal s/n ratio of 10 (low) to 10,000 (high).

Figure 5 shows the uncertainty law results (y-axis) versus the BAYOMA values (given data) for the first four modes. The color bar indicates the level of the modal s/n ratio. It is seen that as the modal s/n ratio increases (from blue to yellow), the c.o.v. decreases; the uncertainty law and BAYOMA values agree better, converging on the 1:1 line.

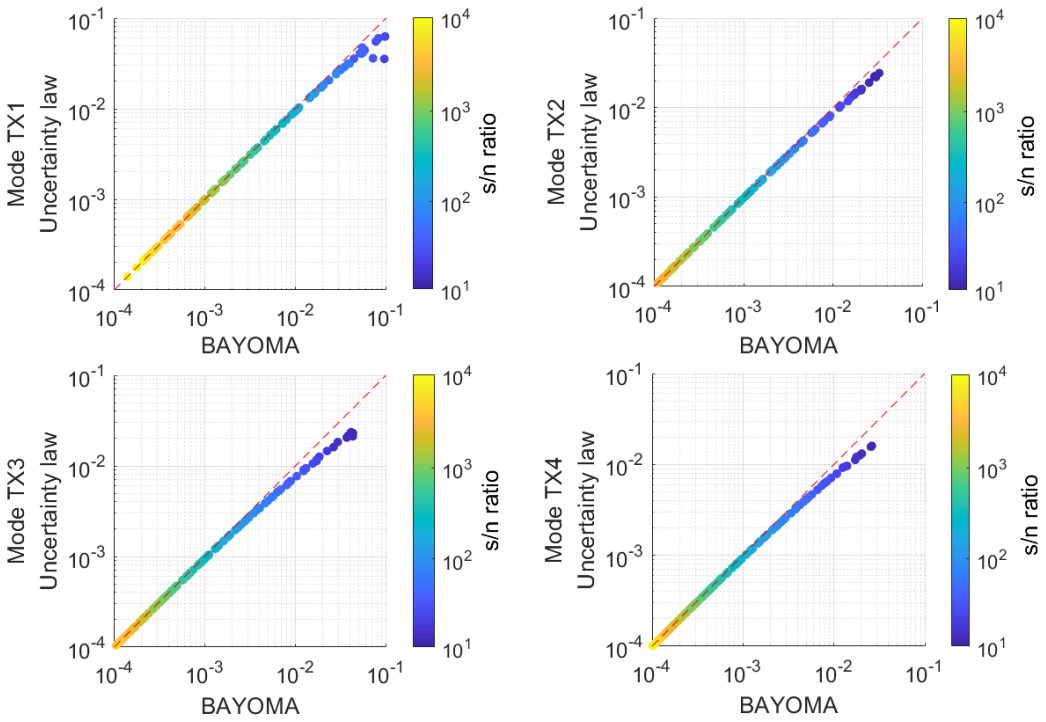

Figure 5. Comparison of mode shape c.o.v. calculated by BAYOMA algorithm (given data) and uncertainty law. Modal s/n ratio is indicated by color; first four modes; synthetic data.

6 Verification with laboratory and field data

Investigation is now extended to laboratory and field data, based on a laboratory-scale shear frame and an eight-storied office building, respectively.

6.1 Laboratory data

Consider a three-storied laboratory shear frame, as shown in Figure 6(a). Each floor is a 30 cm (length) × 20 cm (width) × 3 cm (thickness) aluminum plate with a uniform mass of 4.86 kg. The frame is supported by aluminum bars (dimensions of 22 cm × 1.5 cm × 0.3 cm) fixed at four corners of each floor. The original data set comprises 24 DOFs of biaxial piezoelectric accelerometer measurements at the $3 \times 4 = 12$ corners of the frame. For the study here, we divide the 24 DOFs into two setups, as shown in Figure 6(b). Data was collected at a sampling rate of 2048 Hz and later decimated to 256 Hz for analysis. Figure 7 shows the root SV spectrum of the data in Setup 1. In the resonance band of the mode TX2, although the bottom group of lines suggests a channel noise level below 10 $\mu g/\sqrt{\text{Hz}}$, the (right) tail contribution of TY1 there leads to modeling error (unaccounted mode). Figure 8 and Figure 9 show the c.o.v. of the modal parameters and global mode shape of TX2, analogous to Figure 3 and Figure 4, respectively. Generally, the uncertainty law values (squares) can capture the BAYOMA values (stars) especially for long data, although the scatter can be observed in short data length. This may be attributed to the modeling error from the unaccounted mode just mentioned. As is typical, with real data the c.o.v. (and in fact the MPVs as well) need not follow a smooth trend with data length, due to statistical error and potential modeling error. Similar results can also be observed in other modes (omitted here).

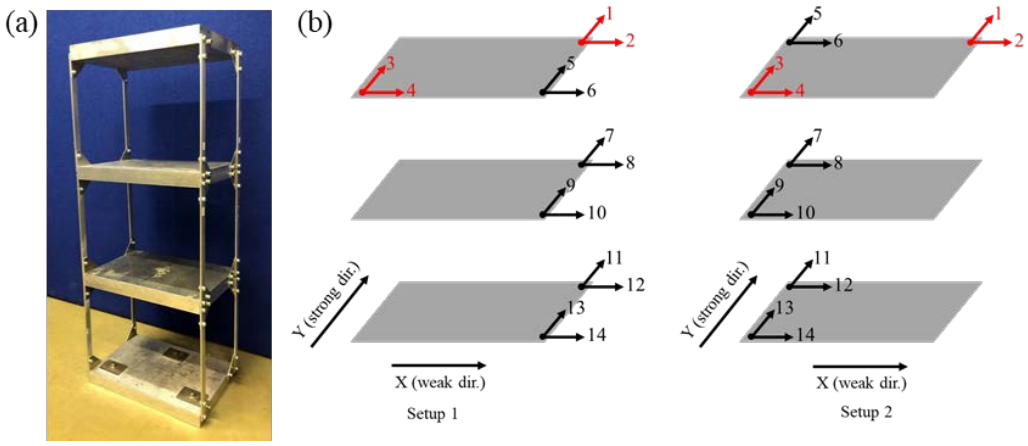

Figure 6. (a) Three-storied aluminum shear frame; (b) setup plan, reference DOFs are colored red.

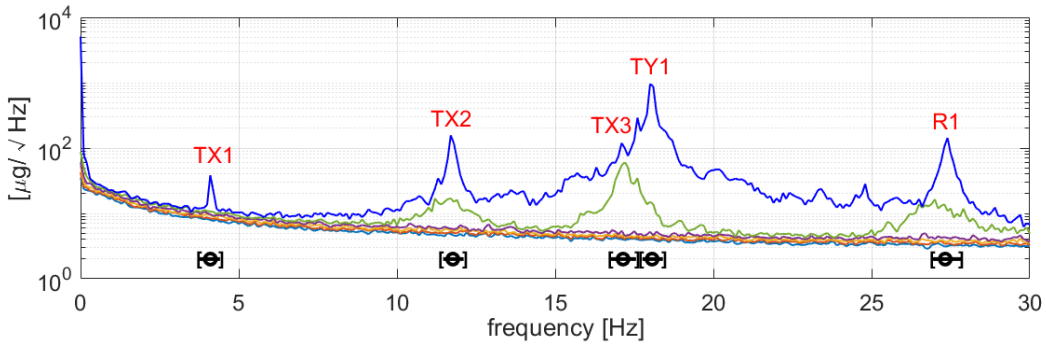

Figure 7. Root SV spectrum with selected frequency bands, based on 300 seconds of data in Setup 1, lab model. TX1 is the first translational mode, R1 is the first rotational mode.

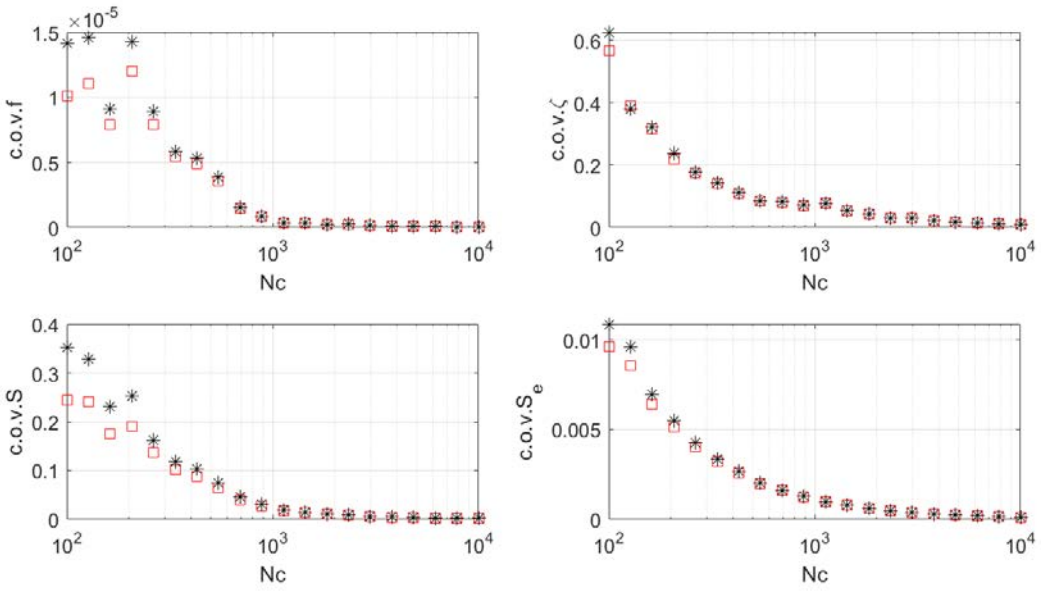

Figure 8. Posterior c.o.v. of modal parameters vs N_c = data length/natural period. Mode TX2, Setup 1, lab model. Same legend as Figure 3.

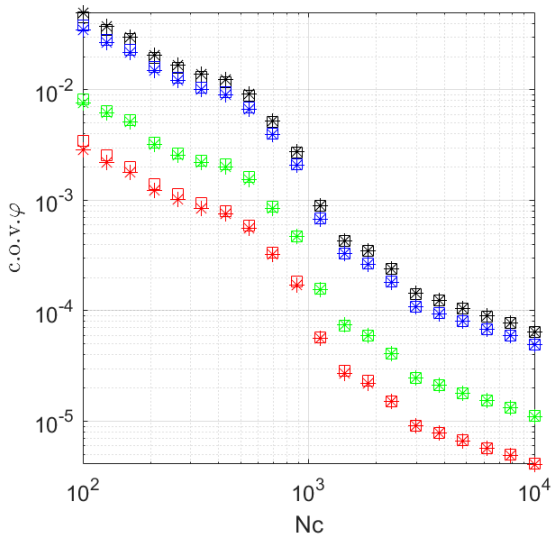

Figure 9. Posterior c.o.v. of global mode shape vs N_c = data length/natural period. Mode TX2, lab model. Same legend as Figure 4.

6.2 Field data

The field data discussed here was collected from the Brodie Tower at the University of Liverpool, which is an eight-storied office building; see Figure 10(a). The same set of data was investigated previously in[38]. Five triaxial servo accelerometers with a noise PSD of about 1 $(\mu g)^2$/Hz were used for the test. Figure 10(b) shows the floor plan with sensor locations. The reference sensor (circled 'R') was deployed at the left corner of the top floor. The rover

sensors (circled numbers) formed a 'T-shape'. The test comprised seven setups, proceeding from the top floor to the bottom. It should be noted that in this study the DOFs of the reference sensor are considered to be different from those measured by sensor 1 in Setup 1, although the two locations are close. Thus, in the context of the proposed theory, the reference DOFs comprise those of the reference sensor (on the top floor); the rover DOFs in Setup 1 comprise those measured by sensors 1 to 4 on the top floor; the rover DOFs in Setup 2 comprise those measured by sensors 1 to 4 on the floor below; and so on. For each setup, ambient vibration data was collected for 20 minutes at a sampling rate of 50 Hz. Figure 11 shows the root SV spectrum of the data in Setup 1. The discussion here focuses on the modes R1 and TY2, which have moderate (about 600) and low (about 20) modal s/n ratios, respectively. The c.o.v.s of modal parameters and global mode shape of R1 are shown in Figure 12 and Figure 13, respectively, which are analogous to Figure 3 and Figure 4. The uncertainty law values (squares) capture well the BAYOMA values (stars) to a similar extent as the synthetic data example. With a low modal s/n ratio and potentially high contribution from unaccounted modes, discrepancy can be observed in the results of TY2 in Figure 14 when the data duration is short.

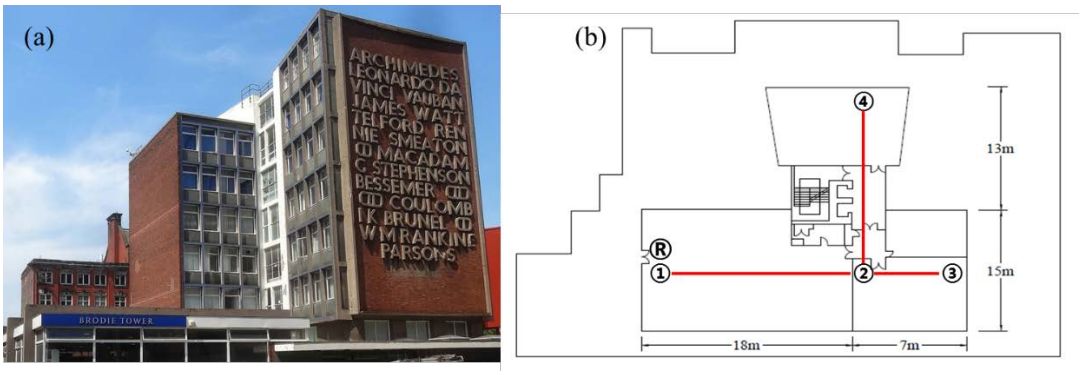

Figure 10. (a) Overview of Brodie Tower; (b) floor plan and sensor locations.

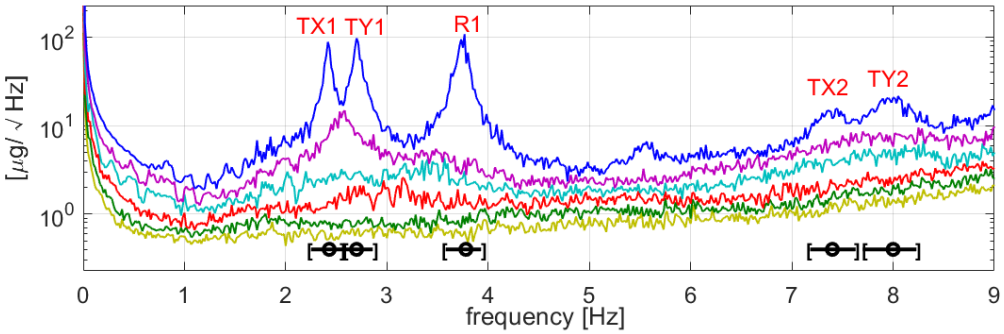

Figure 11. Root SV spectrum with selected frequency bands, Setup 1, Brodie Tower.

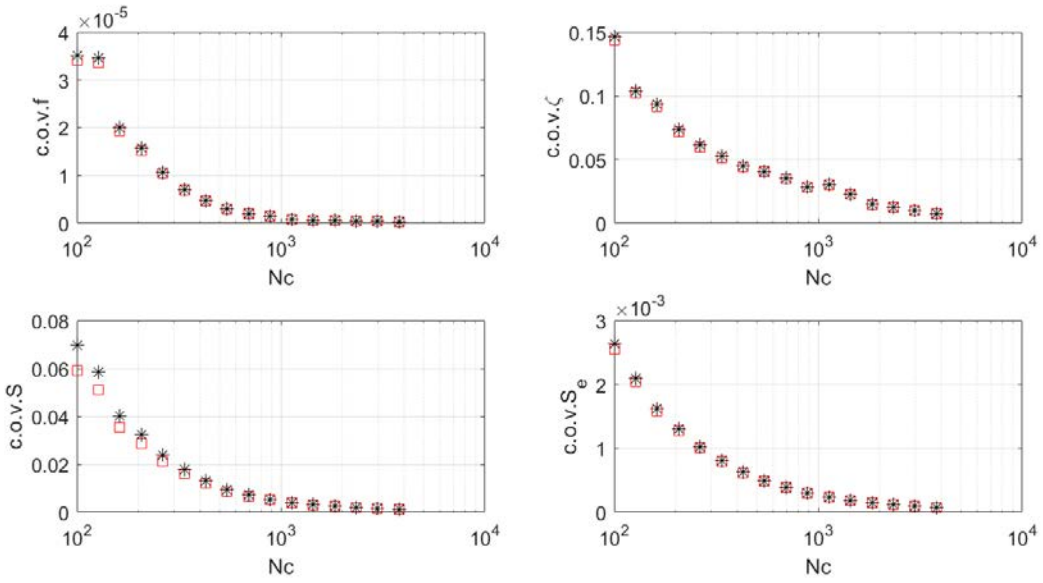

Figure 12 Posterior c.o.v. of modal parameters vs N_c = data length/natural period. Mode R1, Setup 1, Brodie Tower. Same legend as Figure 3.

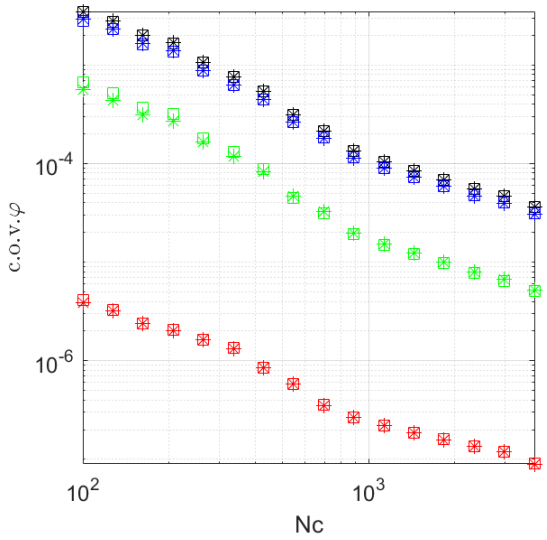

Figure 13. Posterior c.o.v. of global mode shape vs N_c = data length/natural period. Mode R1, Brodie Tower. Same legend as Figure 4.

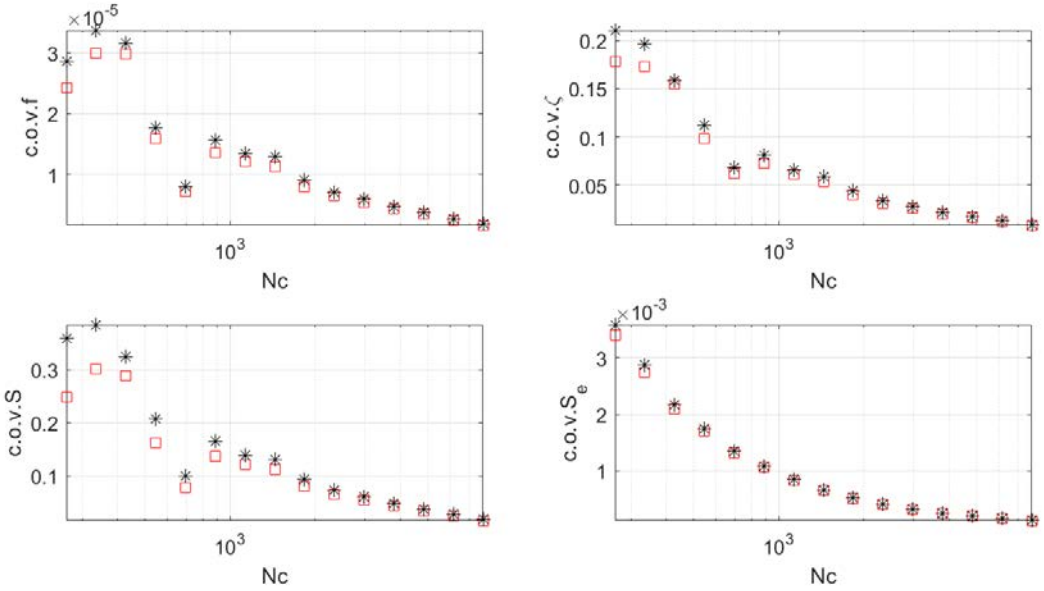

Figure 14. Posterior c.o.v. of modal parameters vs N_c = data length/natural period. Mode TY2, Setup 1, Brodie Tower. Same legend as Figure 3.

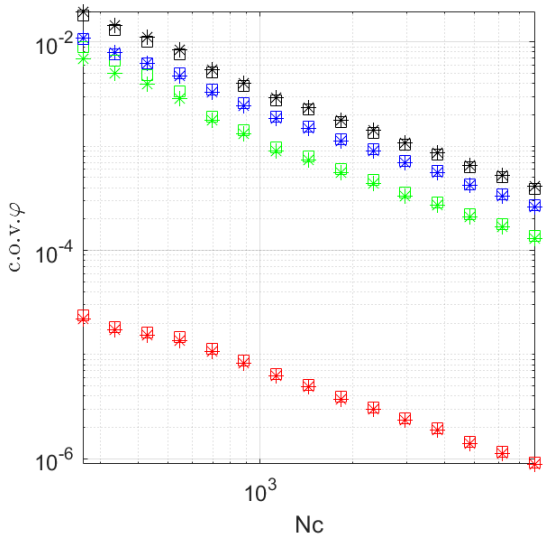

Figure 15. Posterior c.o.v. of the global mode shape vs N_c = data length/natural period. Mode TY2, Brodie Tower. Same legend as Figure 4.

7 Conclusions

This work has discovered the relationship between the identification uncertainty (in terms of c.o.v.) of modal parameters and test configuration for operational modal analysis with multiple setup data. Referred collectively as 'uncertainty law', the results have been derived for a classically damped well-separated mode, long data, small damping, and high modal s/n ratio. Data is assumed to be distributed as the likelihood function, so the results do not

account for modeling error. The uncertainty law reveals that the identification uncertainty of natural frequency and damping ratio in a particular setup is the same as in a single setup setting found previously, i.e., as if other setups were absent. This is not surprising, because they are parameterized separately in different setups and they are asymptotically uncorrelated from local mode shape, which is the only link that connects different setups. Mode shape uncertainty is non-trivial. Focusing on the case of fixed reference and distinct rovers in different setups, the analytical study on the eigenvalue properties of the mode shape covariance matrix reveals that the uncertainty comprises mutually uncorrelated principal directions of local and global nature. While both local and global types of uncertainty depend on modal s/n ratios, only those of global nature depends on sensor locations through the partial mode shape norms of reference DOFs and rover DOFs in each setup. The proposed theory has been validated using synthetic, laboratory and field data. The uncertainty law presented provides the basis for planning multiple setup ambient vibration tests taking into account identification uncertainty. By virtue of the Cramer-Rao bound, up to the same modeling assumptions, the uncertainty law gives the lower bound of identification uncertainty and hence dictates the achievable precision limit of OMA regardless of identification method [36]. Although the theory has been developed assuming acceleration data, it is applicable for data of other kinematic types (e.g., velocity). This follows from the same argument for single setup data; e.g., see Section 16.6 of [24].

Advancing the state of knowledge, recently discovered uncertainty law for close modes [32–34] identified with single setup data reveals that the insights generated in this paper is unlikely to carry over directly to close modes with multiple setup data. Mode shapes of close modes have an uncertainty within the mode shape subspace that does not vanish even for noiseless data and that correlates with all parameters. This uncertainty is not found in well-separated modes, exhibiting the complexity of modal entangling and another level of challenge.

8 Acknowledgments

This work is part of a research project on ‘‘Uncertainty quantification and management in ambient modal identification” funded by the Engineering and Physical Sciences Research Council, UK (grant EP/N017897/1) to understand identification uncertainty and provide a strong scientific basis for implementing and planning ambient vibration tests. Part of the work was performed during the PhD of the first author at the University of Liverpool with a

scholarship from the Chinese Scholarship Council, China. Currently, the first and third author are funded by Start-up Grant 130000-171207704/018 from Zhejiang University; and the second author by Start-up Grant M4082398 at NTU. These financial supports are gratefully acknowledged.

9 Supplementary data

The research materials supporting this publication can be accessed by contacting yanlongxie@zju.edu.cn.

Appendix A: Expressions for partitions of $\boldsymbol{J}$

This appendix derives the expressions of the partitions of $\boldsymbol{J}$ in (22) to (24). As in Sections 3.3 and 4.2, it is assumed that the reference DOFs are fixed and rover DOFs are distinct in different setups. Also, in any given setup a DOF is measured by at most one data channel. Let $\boldsymbol{B}_R$ $(n_R \times n)$ and $\boldsymbol{B}_i$ $(n_{vi} \times n)$ be selection matrices that pick from the global mode shape the reference DOFs and the rover DOFs in Setup i, respectively, i.e.,

$$\boldsymbol{u}_R = \boldsymbol{B}_R\boldsymbol{\varphi} \qquad \boldsymbol{u}_i = \boldsymbol{B}_i\boldsymbol{\varphi} \tag{47}$$

The partitions of $\boldsymbol{J}$ appearing in (20) and (21) can then be written as

$$\boldsymbol{J}_{RR} = \boldsymbol{B}_R\boldsymbol{J}\boldsymbol{B}_R^T \qquad \boldsymbol{J}_{ii} = \boldsymbol{B}_i\boldsymbol{J}\boldsymbol{B}_i^T \qquad \boldsymbol{J}_{Ri} = \boldsymbol{B}_R\boldsymbol{J}\boldsymbol{B}_i^T \tag{48}$$

Substituting $\boldsymbol{J}$ in (6) into the expression of $\boldsymbol{J}_{RR}$ gives

$$\boldsymbol{J}_{RR} = \sum_i k_i\boldsymbol{B}_R\boldsymbol{L}_i^T\left(\boldsymbol{I} - \overline{\boldsymbol{v}}_i\overline{\boldsymbol{v}}_i^T\right)\boldsymbol{L}_i\boldsymbol{B}_R^T = \sum_i k_i\left[\boldsymbol{B}_R\boldsymbol{L}_i^T\boldsymbol{L}_i\boldsymbol{B}_R^T - \left(\boldsymbol{B}_R\boldsymbol{L}_i^T\overline{\boldsymbol{v}}_i\right)\left(\boldsymbol{B}_R\boldsymbol{L}_i^T\overline{\boldsymbol{v}}_i\right)^T\right] \tag{49}$$

It can be reasoned that $\boldsymbol{L}_i^T\boldsymbol{L}_i$ is a $n \times n$ diagonal matrix whose jth diagonal entry is equal to the number of data channels in Setup i measuring DOF j. The matrix $\boldsymbol{B}_R\boldsymbol{L}_i^T\boldsymbol{L}_i\boldsymbol{B}_R^T$ is then a diagonal matrix where the jth diagonal entry is equal to the number of channels in Setup i measuring reference DOF j. Under the assumptions stated in the beginning, every reference DOF is measured in all setups by exactly one data channel, and so the diagonal entries are all equal to 1, implying that $\boldsymbol{B}_R\boldsymbol{L}_i^T\boldsymbol{L}_i\boldsymbol{B}_R^T$ is a $n_R \times n_R$ identity matrix. On the other hand, $\boldsymbol{L}_i^T\overline{\boldsymbol{v}}_i$ $(n_R \times n_i)$ puts the measured DOFs of $\overline{\boldsymbol{v}}_i$ to an expanded $n \times 1$ vector. Every entry in this vector is equal to the mode shape value multiplied by the number of times the DOF is

measured in Setup i. Since a DOF is measured by at most one channel in a given setup, the entry is either equal to zero (when the DOF is not measured in Setup i) or otherwise the mode shape value. As the same n_R reference DOFs are measured in all setups, the $n_R \times 1$ vector $\boldsymbol{B}_R \boldsymbol{L}_i^T \overline{\boldsymbol{v}}_i$ collects the mode shape values of the refence DOFs, i.e., $\boldsymbol{B}_R \boldsymbol{L}_i^T \overline{\boldsymbol{v}}_i = \boldsymbol{u}_R / \|\boldsymbol{v}_i\|$. The above considerations imply $\boldsymbol{J}_{RR} = \Sigma_j k_j \left(\boldsymbol{I} - b_j^{-1} \boldsymbol{u}_R \boldsymbol{u}_R^T\right)$ as in (22), where $b_j = \left\|\boldsymbol{v}_j\right\|^2$. Under the same assumptions, it can be reasoned in a similar manner that $\boldsymbol{J}_{ii} = k_i \left(\boldsymbol{I} - b_i^{-1} \boldsymbol{u}_i \boldsymbol{u}_i^T\right)$ as in (23), where only the ith term in (6) contributes because the rover DOFs in different setups are distinct. Also, $\boldsymbol{J}_{Ri} = -k_i b_i^{-1} \boldsymbol{u}_R \boldsymbol{u}_i^T$ as in (24), where the identity matrix in (6) disappears because $\boldsymbol{J}_{Ri}$ corresponds to an off-diagonal partition.

Appendix B: Constrained Hessian of $\boldsymbol{\delta_G^2}$

In this appendix we show that the Hessian of δ_G^2 in (43) at $\boldsymbol{c} = \hat{\boldsymbol{c}}$ in (46) under the mode shape norm constraint $c_R + \Sigma_i c_i = 1$ is negative semi-definite. Let the constraint be specified as the scalar equation $g(\boldsymbol{c}) = 0$ and $\boldsymbol{v}(\boldsymbol{c})$ be a function that maps $\boldsymbol{c}$ to a $n_s \times 1$ vector that always satisfies the constraint, i.e., $g\big(\boldsymbol{v}(\boldsymbol{c})\big) = 0$ for any $\boldsymbol{c}$. The Hessian of δ_G^2 under constraint can then be determined as the Hessian of the composite function $\delta_G^2(\boldsymbol{v}(\boldsymbol{c}))$ with respect to $\boldsymbol{c}$. At the stationary point $\boldsymbol{c} = \hat{\boldsymbol{c}}$, this 'constrained Hessian' is given by [39]

$$\boldsymbol{H} = \left(\frac{\partial \hat{v}}{\partial c}\right)^T \left(\frac{\partial^2 \hat{\delta}_G^2}{\partial c^2} + \hat{\mu} \frac{\partial^2 \hat{g}}{\partial c^2}\right) \left(\frac{\partial \hat{v}}{\partial c}\right) \tag{50}$$

where a hat '^' denotes that the derivative is evaluated at $\boldsymbol{c} = \hat{\boldsymbol{c}}$; $\hat{\mu}$ is the Lagrange multiplier obtained in (46). The choice of $\boldsymbol{v}$ and g is not unique but $\boldsymbol{H}$ is invariant to the choice. For the purpose here we take

$$g(\boldsymbol{c}) = 1 - c_R - \Sigma_i c_i \qquad \boldsymbol{v} = \begin{bmatrix} v_1 \\ \vdots \\ v_{n_s} \end{bmatrix} \qquad v_i = c_i - \bar{c} + n_s^{-1}(1 - c_R) \tag{51}$$

where $\bar{c} = \Sigma_i c_i / n_s$ is the mean of $\{c_i\}_{i=1}^{n_s}$. Note that

$$g(\boldsymbol{v}) = 1 - c_R - \Sigma_i v_i = 1 - c_R - (\Sigma_i c_i - n_s \bar{c} + 1 - c_R) = 0 \tag{52}$$

and so $\boldsymbol{v}(\boldsymbol{c})$ satisfies the norm constraint for any $\boldsymbol{c}$. Direct differentiation gives

$$\frac{\partial^2 \delta_G^2}{\partial c^2} = c_R^{-1}\boldsymbol{A} \qquad \frac{\partial^2 g}{\partial c^2} = \mathbf{0} \qquad \frac{\partial v}{\partial c} = \boldsymbol{I} - n_s^{-1}\mathbf{1}\mathbf{1}^T \tag{53}$$

where $\mathbf{1} = [1, \dots, 1]^T$ denotes a column vector of ones. Substituting (50) into gives

$$\boldsymbol{H} = c_R^{-1}(\boldsymbol{I} - n_s^{-1}\mathbf{1}\mathbf{1}^T)\boldsymbol{A}(\boldsymbol{I} - n_s^{-1}\mathbf{1}\mathbf{1}^T) \tag{54}$$

To proceed, we rewrite $\boldsymbol{A}$ in (44) as

$$\boldsymbol{A} = \boldsymbol{s}\mathbf{1}^T + \mathbf{1}\boldsymbol{s}^T - 2diag(\boldsymbol{s}) \tag{55}$$

where $\boldsymbol{s} = \left[s_1, \dots, s_{n_s}\right]^T$, $s_i = k_i^{-1}$ and $diag(\boldsymbol{s})$ denotes a diagonal matrix of the entries in $\boldsymbol{s}$. Substituting into (54) and simplifying gives

$$\boldsymbol{H} = 2c_R^{-1}n_s^{-1}[\boldsymbol{s}\mathbf{1}^T + \mathbf{1}\boldsymbol{s}^T - n_s diag(\boldsymbol{s}) - \bar{s}\mathbf{1}\mathbf{1}^T] \tag{56}$$

where $\bar{s} = \Sigma_i k_i^{-1}/n_s$. For any $\boldsymbol{x} = \left[x_1, \dots, x_{n_s}\right]^T$, direct algebra gives

$$\boldsymbol{x}^T\boldsymbol{H}\boldsymbol{x} = 2c_R^{-1}\left(2\bar{x}\Sigma_i s_i x_i - \Sigma_i s_i x_i^2 - n_s\bar{s}\bar{x}^2\right) = 2c_R^{-1}n_s\bar{s}\left(2\bar{x}\Sigma_i w_i x_i - \Sigma_i w_i x_i^2 - \bar{x}^2\right) \tag{57}$$

where $\bar{x} = n_s^{-1}\sum_j x_j$ and $w_i = s_i/\Sigma_j s_j$ $(i = 1, \dots, n_s)$ can be viewed as positive weights that sum to unity. Denoting the weighted mean by $\bar{y} = \Sigma_i w_i x_i$ and using the standard result $\Sigma_i w_i x_i^2 \geq (\Sigma_i w_i x_i)^2 = \bar{y}^2$ (mean square is bounded below by square of mean),

$$\boldsymbol{x}^T\boldsymbol{H}\boldsymbol{x} \leq 2c_R^{-1}n_s\bar{s}(2\bar{x}\bar{y} - \bar{y}^2 - \bar{x}^2) = -2c_R^{-1}n_s\bar{s}(\bar{x} - \bar{y})^2 \leq 0 \tag{58}$$

As this holds for any $\boldsymbol{x}$, it follows that $\boldsymbol{H}$ is negative semi-definite.

References

[1] B. Peeters, G. De Roeck, Stochastic system identification for operational modal analysis: A review, J. Dyn. Syst. Meas. Control. 123 (2001) 659–667.

[2] R. Brincker, C. Ventura, Introduction to operational modal analysis, Wiley, London, 2015.

[3] L. Hermans, H. Van Der Auweraer, Modal testing and analysis of structures under operational conditions: industrial applications, Mech. Syst. Signal Process. 13 (1999) 193–216.

[4] S.S. Ivanovic, M.D. Trifunac, M.I. Todorovska, Ambient vibration tests of structure-a review, J. Earthq. Tecknology. 37 (2000) 165–197.

[5] D.M. Siringoringo, Y. Fujino, System identification of suspension bridge from ambient vibration response, Eng. Struct. 30 (2008) 462–477.

[6] W. Shi, J. Shan, X. Lu, Modal identification of Shanghai World Financial Center both from free and ambient vibration response, Eng. Struct. 36 (2012) 14–26.

[7] J.M.W. Brownjohn, F. Magalhaes, E. Caetano, A. Cunha, Ambient vibration re-testing and operational modal analysis of the Humber Bridge, Eng. Struct. 32 (2010) 2003–2018.

[8] M.E. Friswell, J.E. Mottershead, Finite element updating in structural dynamics, Springer Netherlands, Dordrecht, 1999.

[9] K.V. Yuen, L.S. Katafygiotis, Bayesian fast fourier transform approach for modal updating using ambient data, Adv. Struct. Eng. 6 (2003) 81–95.

[10] Y. Xia, H. Hao, J.M.W. Brownjohn, P.Q. Xia, Damage identification of structures with uncertain frequency and mode shape data, Earthq. Eng. Struct. Dyn. 31 (2002) 1053–1066.

[11] H.F. Lam, J. Yang, Bayesian structural damage detection of steel towers using measured modal parameters, Earthq. Struct. 8 (2015) 935–956.

[12] J.M.W. Brownjohn, Structural health monitoring of civil infrastructure, Philos. Trans. R. Soc. A Math. Phys. Eng. Sci. 365 (2007) 589–622.

[13] S. Cho, H. Jo, S. Jang, J. Park, H.J. Jung, C.B. Yun, B.F. Spencer, J.W. Seo, Structural health monitoring of a cable-stayed bridge using wireless smart sensor technology: Data analyses, Smart Struct. Syst. 6 (2010) 461–480.

[14] F. Magalhães, A. Cunha, E. Caetano, Vibration based structural health monitoring of an arch bridge: From automated OMA to damage detection, Mech. Syst. Signal Process. 28 (2012) 212–228.

[15] E. Reynders, F. Magalhaes, G. De Roeck, A. Cunha, Merging strategies for multi-setup operational modal analysis: application to the Luiz I steel arch bridge, in: Proc. IMAC, 2009.

[16] M. Dohler, E. Reynders, F. Magalhaes, L.Mevel, G. De Reock, A. Cunha, Pre and post identification merging for multi setup OMA with covariance driven SSI, in: IMAC-XXVIII, 2010: pp. 57–70.

[17] S.K. Au, Assembling mode shapes by least squares, Mech. Syst. Signal Process. 25 (2011) 163–179.

[18] L. Mevel, M. Basseville, A. Benveniste, M. Goursat, Merging sensor data from multiple

measurement set-ups for non-stationary subspace-based modal analysis, J. Sound Vib. 249 (2002) 719–741.

[19] E. Reynders, R. Pintelon, G.D. Roeck, Uncertainty bounds on modal parameters obtained from stochastic subspace identification, Mech. Syst. Signal Process. 22 (2007) 948–969.

[20] P. Andersen, R. Brincker, Estimation of modal parameters and their uncertainties, 17th Int. Modal Anal. Conf. 1 (1999) 323–329.

[21] M. Döhler, X.B. Lam, L. Mevel, Uncertainty quantification for modal parameters from stochastic subspace identification on multi-setup measurements, Mech. Syst. Signal Process. 36 (2013) 562–581.

[22] M. El-kafafy, T. De Troyer, B. Peeters, P. Guillaume, Fast maximum-likelihood identification of modal parameters with uncertainty intervals: A modal model-based formulation, Mech. Syst. Signal Process. 37 (2013) 422–439.

[23] R. Pintelon, P. Guillaume, J. Schoukens, Uncertainty calculation in (operational) modal analysis, Mech. Syst. Signal Process. 21 (2007) 2359–2373.

[24] S.K. Au, Operational modal analysis: modeling, Bayesian inference, uncertainty laws, Springer, Singapore, 2017.

[25] S.K. Au, Fast Bayesian FFT method for ambient modal identification with separated modes, J. Eng. Mech. 137 (2011) 214–226.

[26] S.K. Au, F.L. Zhang, Fast Bayesian ambient modal identification incorporating multiple setups, J. Eng. Mech. 138 (2012) 800–815.

[27] F.L. Zhang, S.K. Au, H.F. Lam, Assessing uncertainty in operational modal analysis incorporating multiple setups using a Bayesian approach, Struct. Control Heal. Monit. 22 (2014) 395–416.

[28] S.K. Au, Uncertainty law in ambient modal identification, Part I: Theory, Mech. Syst. Signal Process. 48 (2014) 15–33.

[29] S.K. Au, J.M.W. Brownjohn, J.E. Mottershead, Quantifying and managing uncertainty in operational modal analysis, Mech. Syst. Signal Process. 102 (2018) 139–157.

[30] J.M.W. Brownjohn, S.K. Au, B. Li, J. Bassitt, Optimised ambient vibration testing of long span bridges, Procedia Eng. 199 (2017) 38–47.

[31] J.M.W. Brownjohn, S.K. Au, Y. Zhu, Z. Sun, B. Li, J. Bassitt, E. Hudson, H. Sun, Bayesian operational modal analysis of Jiangyin Yangtze River Bridge, Mech. Syst. Signal Process. 110 (2018) 210–230.

[32] S.K. Au, J.M.W. Brownjohn, B. Li, A. Raby, Understanding and managing identification uncertainty of close modes in operational modal analysis, Mech. Syst. Signal Process.

147 (2021) 107018. doi:10.1016/j.ymssp.2020.107018.

[33] S.K. Au, J.M.W. Brownjohn, Asymptotic identification uncertainty of close modes in Bayesian operational modal analysis, Mech. Syst. Signal Process. 133 (2019) 106273. doi:10.1016/j.ymssp.2019.106273.

[34] S.K. Au, B. Li, J.M.W. Brownjohn, Achievable precision of close modes in operational modal analysis: Wide band theory, Mech. Syst. Signal Process. (2020) 107016. https://doi.org/10.1016/j.ymssp.2020.107016.

[35] D.R. Brillinger, Time series: data analysis and theory, Siam, Philadelphia, 1981. doi:http://dx.doi.org/10.1137/1.9780898719246.

[36] S.K. Au, B. Li, Posterior uncertainty, asymptotic law and Cramér-Rao bound, Struct. Control Heal. Monit. 25 (2018) 1–21.

[37] Y.L. Xie, Uncertainty quantification and management in operational modal analysis with multiple setups, University of Liverpool, 2018.

[38] Y.C. Zhu, Y.L. Xie, S.K. Au, Operational modal analysis of an eight-storey building with asynchronous data incorporating multiple setups, Eng. Struct. 165 (2018) 50–62.

[39] S.K. Au, Y.L. Xie, Calculation of Hessian under constraints with applications to Bayesian system identification, Comput. Methods Appl. Mech. Eng. 323 (2017) 373–388.